THE JOHNS HOPKINS UNIVERSITY

DEPARTMENT OF PHYSICS

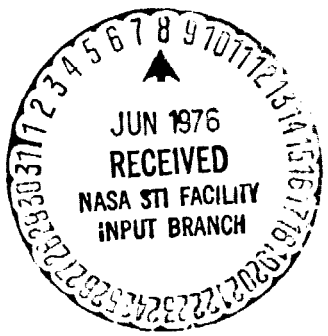

MULTIPLE DETECTOR FOCAL PLANE ARRAY ULTRAVIOLET SPECTROMETER FOR THE AMPS LABORATORY

Final Report

Contract NAS 8-31413

Submitted by

Paul D. Feldman

November 30, 1975

Baltimore, Maryland 21218

MULTIPLE DETECTOR FOCAL PLANE ARRAY ULTRAVIOLET SPECTROMETER FOR THE AMPS LABORATORY

Final Report

Contract NAS 8-31413

Paul D. Feldman
Physics Department
The Johns Hopkins University
Baltimore, Maryland 21218

November 30, 1975

I. Introduction

In more than 15 years of use in rockets and satellites ultraviolet spectroscopy has proved to be one of the leading tools in the study of atmospheric science, both in terms of the earth's upper atmosphere as well as the atmospheres of planets and comets. Over this period of time, the instruments used have evolved from the large rocket-borne scanning spectrometers used to first measure the ultraviolet emissions of the terrestrial airglow and aurora (Fastie et al., 1964) to the most recent miniaturized spectrometers included in planetary probes to Venus, Mercury and Jupiter that are in many cases more sensitive than the original large rocket instruments. The development of these modern instruments was made possible by the rapid progress in the development of detector technology, pulse counting electronics using integrated circuit technology, and improvements in the art of ruling diffraction gratings. Most recently, much attention has been directed to the development of multi-element pulse counting detectors for the vacuum ultraviolet, which would combine the large information content of photographic film recording with the high efficiency and quantum detection limit of single pulse counting that can be achieved with individual photomultiplier tubes.

An array of ultraviolet and visible spectrometers will be part of the core instrumentation of the AMPS payloads to be flown on Spacelab missions beginning in the early 1980's. The ultraviolet region of the spectrum, and the vacuum ultraviolet (300-2000 A) in particular,

is perhaps the most important for atmospheric science since the principal radiative transitions of the neutral atoms, ions and molecules of the most abundant atmospheric constituents occur in this region. For AMPS the spectroscopic instrumentation must be capable not only of observation of the quiescent or magnetically disturbed atmosphere, but also of observation of transient events induced by on-board accelerators, lasers or chemical releases. Thus, the requirements for the AMPS spectrometers can be written in terms of spectral, spatial and temporal resolution, with particular combinations of these parameters for any particular experiment. In addition, the power, weight and volume limitations associated with satellite and probe experiments are not a restriction for the AMPS instrumentation, so that flexibility can be coupled with increased sensitivity simply by using the state-of-the-art detector technology with large aperture instrumentation.

The present study examines the possibility of achieving these aims using a multi-element focal plane detector array in a conventional spectrograph mount. The requirements on the detector array are determined from the optical design of the spectrometer which in turn depends on the desired level of resolution and sensitivity required. The choice of available detectors and their associated electronics and controls is surveyed, and it is to be borne in mind that the data collection rate from this system is so great that on-board processing and reduction of data are absolutely essential. Finally, we will look

at parallel developments in instrumentation for imaging in astronomy, both in the ultraviolet (for the Large Space Telescope as well as other rocket and satellite programs) and in the visible to determine what progress in that area can have direct bearing on atmospheric spectroscopy.

II. Spectrometer Design

A. Viewing geometry. With the exception of those emissions produced in the vicinity of the Spacelab by experiments on board, most of the radiation to be observed will be produced at altitudes considerably below the orbital altitude of the Space Shuttle (here taken to be in the range of 250-400 km). A particularly useful means of observation in this case is a limb-viewing geometry using an auxiliary telescope as illustrated in Fig. 1a. For a spectrometer at altitude z_o, an element of the slit area (projected through the telescope at an angle θ_e below the local horizontal) will receive most of its radiation along its line of sight from the tangent point at altitude z_e, a distance x from the spacecraft:

$$z_e = (z_o + R_e) \cos \theta_e - R_e , \tag{1}$$

$$x = (z_o + R_e) \sin \theta_e , \tag{2}$$

where R_e is the radius of the earth. If now, a slit of length ℓ is oriented so as to be projected vertically onto the limb (Fig. 1b),

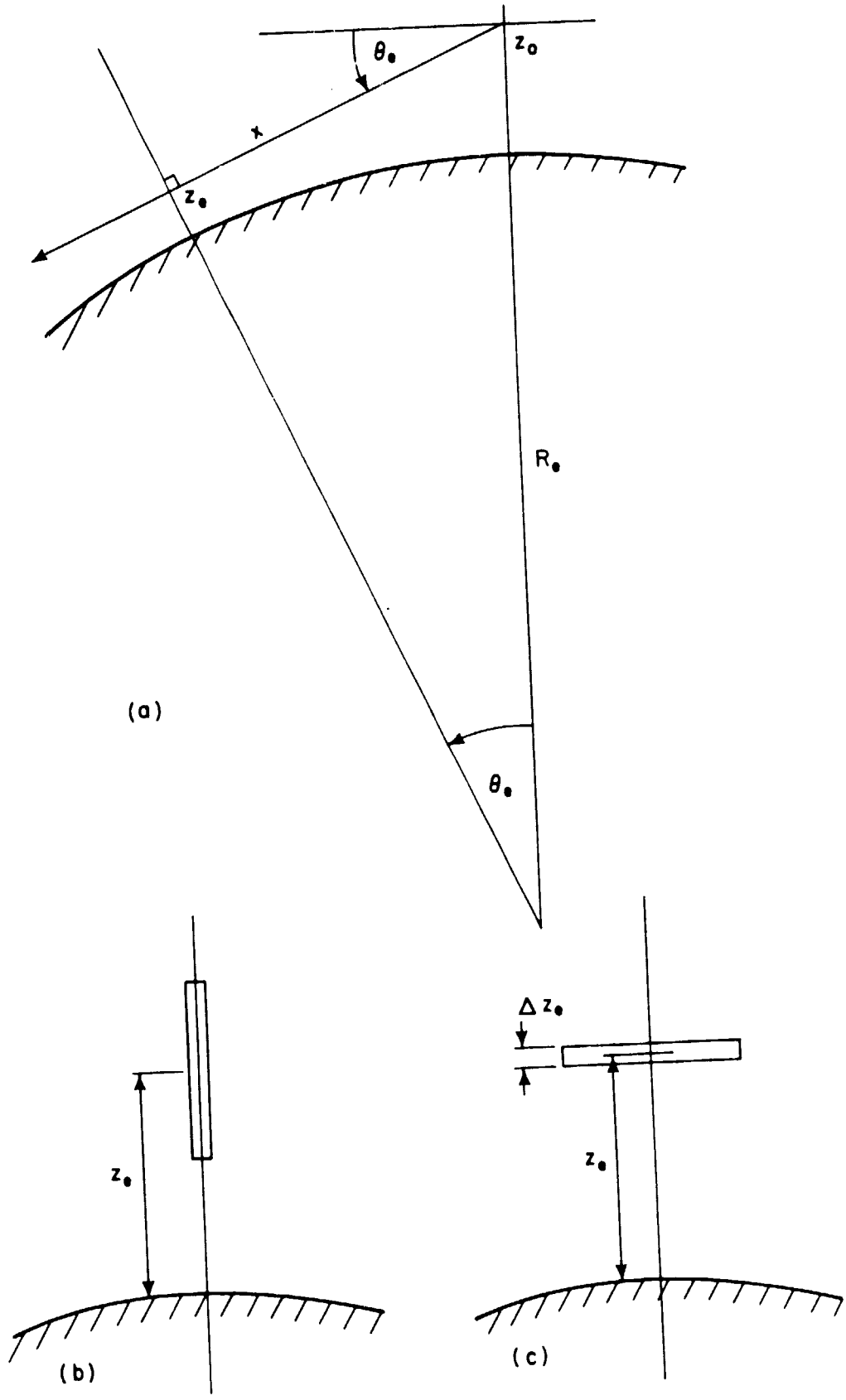

Fig. 1. Limb viewing geometry

each point on the slit will image a different tangent altitude according to Eq. 1. For a telescope of focal length F, an element of slit length Δy will image a vertical height element Δz_e given by:

$$\Delta z_e = (z_o + R_e) \sin \theta_e \frac{\Delta y}{F} \tag{3}$$

Finally, if we image this slit onto the exit focal plane of the spectrometers, we produce the two-dimensional image, Fig. 2, in which the spatial and spectral dispersion appear orthogonal to each other. Note that Eq. 3 contains the pointing accuracy requirement if Δz_e is taken to be the spatial resolution element since then $\Delta\theta_e = \frac{\Delta y}{F}$ would be the stability needed. It is important to know the spectrometer attitude to this accuracy, which typically is of the order of a few arc minutes, even though it may not be possible to actually point the spectrometer to this accuracy.

Telescope parameters will depend on the optical details of the spectrometer, but in general the focal length will be chosen to image a fraction to several atmospheric scale heights onto the slit length, while the f-number should match that of the spectrometer collimator. There are instances in which the telescope will not be used so that it should be mechanically removable from the spectrometer assembly. The telescope is also useful to provide in-flight calibration through the observation of a set of standard ultraviolet reference stars (Henry et al., 1975).

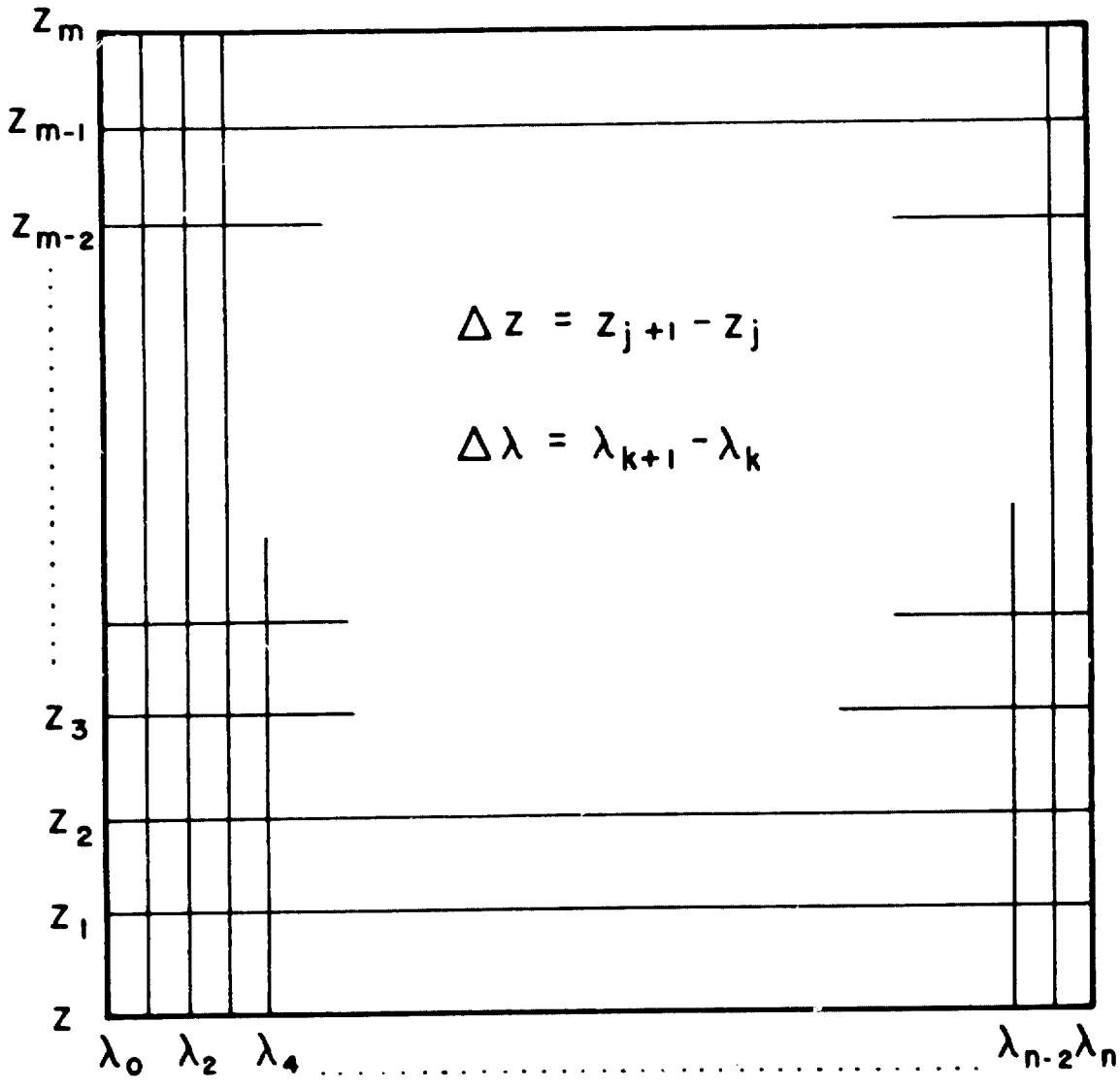

Fig. 2. Focal plane image for viewing geometry of Fig. 1b

B. Ebert-Fastie Mount

For all spectral ranges longward of 1100 A, the Ebert-Fastie configuration offers the advantage of a fast compact spectrometer mount with maximum mechanical stability. The basic layout is shown in Fig. 3. There are only two optical components - a plane grating and a truncated spherical mirror. By proper choice of the distance of the grating axis to the vertex of the mirror (approximately 0.4 of the mirror radius of curvature) the focal plane will be flat enabling the use of a plane multi-element detector at the exit. For purposes of illustration, the figure, and the calculations to follow, we assume a spectrometer focal length, F, of 0.5 m (1.0 m radius of curvature) and a detector array 25 mm x 25 mm (a standard vidicon size).

The spectral dispersion, and hence the grating ruling, depends on the spectral range that it is desired to span with a detector of given width (Fig. 2). In practice, the grating is fixed with its normal at an angle θ to the mirror axis. The incident and diffracted rays make angles with the grating normal, α and β respectively, where

$$\alpha = \theta - \phi_1$$

$$\beta = \theta + \phi_2$$

and ϕ_1 and ϕ_2 are the respective angles of the incident and diffracted rays with the mirror axis (see Fig. 3). The grating equation for the n^{th} order is then

$$n\lambda = d(\sin\alpha + \sin\beta) \qquad (4)$$

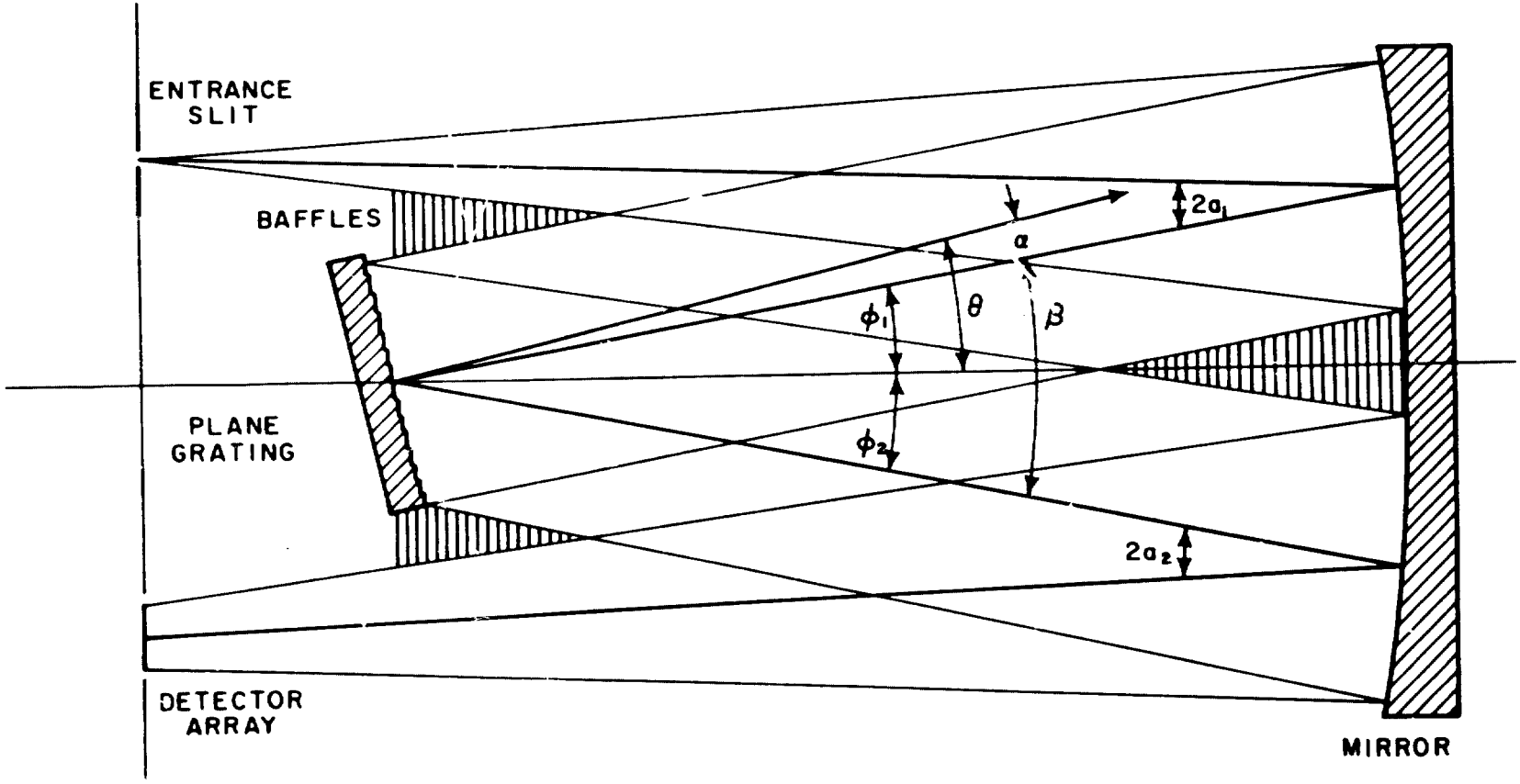

Fig. 3. Optical diagram of the Ebert-Fastie spectrometer

which in the case of $\phi_1 = \phi_2 = \phi$ becomes $n\lambda = 2d \sin\theta \cos\phi$ and the dispersion, D_λ, in the focal plane is

$$n \frac{d\lambda}{dx} = \frac{d}{F} \cos\beta \equiv nD_\lambda \tag{5}$$

where d is the grating spacing. Analagously, we can define a spatial dispersion, D_z, in the direction normal to the spectral dispersion by rewriting Eq. 3 as

$$\frac{dz_e}{dy} = \frac{(z_o + R_e)}{F} \sin\theta_e \equiv D_z \tag{6}$$

Equations 5 and 6 now define the imaging properties of the spectrometer and the resolution, both spatial and spectral, will be limited by the optical aberrations.

C. Aberrations

The principal aberrations in the Ebert configuration are astigmatism and coma (Fastie, 1952), and these will be most severe in the four corners of the detector field. The length of the astigmatic image of a point on the slit can be calculated using Coddington's Equations (Strong, 1958) to compute the image distances $s'_\parallel$ and $s'_\perp$ of the parallel and perpendicular images, respectively. The separation between these images can be written simply in terms of a_1, the angle between the central ray and the mirror normal (Fig. 3):

$$\Delta s' = s'_\parallel - s'_\perp = a_1^2 F \tag{7}$$

from which the image length $\Delta\ell'$ is given in terms of the f/number of the system by

$$\Delta\ell' = \frac{\Delta s'}{f} \tag{8}$$

Coma at the center of the detector can be made to vanish if the angles α, β, a_1 and a_2 satisfy

$$\frac{a_1}{a_2} = \frac{\cos^3 \beta}{\cos^3 \alpha} \tag{9}$$

where a_2 now refers to the ray passing through the center of the detector (Shafer et al., 1963). The coma at the edge of detector (of width w) can be shown to be

$$\delta = \frac{3}{16} \cdot \frac{w}{2f^2} \tag{10}$$

For the 0.5 m focal length spectrometer of Fig. 3, $\phi_1 = 10.1^o$, $\phi_2 = 11.3^o$, $a_1 = 0.11$, $a_2 = 0.12$, the astigmatism is 0.6 mm in the direction of the slit length, while the maximum coma is 0.1 mm in the direction of the dispersion. For points not on the central plane the astigmatic image is curved and at the ends of the slit the spread in the direction of the dispersion is comparable to the coma. This now defines the detector element size $\Delta y \times \Delta x$ and consequently the spectral resolution $\Delta\lambda = \Delta x \cdot D_\lambda$ and the spatial resolution $\Delta z_e = \Delta y \cdot D_z$. The number of detector elements for a square array of side w is then $w^2/\Delta x \Delta y$.

D. Spectral Resolution

In practice one would not have a single detector element equal to the spectral or spatial resolution element, but rather three or more detector elements would span the half-width (FWHM) of the instrument response function or the altitude function. Note that it is always possible to operate at a poorer resolution by electronically summing adjacent detector elements in one or both dimensions so as to produce "new" elements of integral multiples of the basic element size. At the same time the entrance slit could be mechanically opened to achieve the increased sensitivity obtained with the reduction in resolving power.

At the highest desired spectral resolution, it will not be possible to observe at any one time the entire spectral range that a given photocathode is sensitive to. Thus the grating position (i.e., the angle θ) will have to be adjustable and programmable according to each individual experimenter's needs. In fact, in order to provide the entire range of spectral resolution required will most likely require more than one grating, and a straightforward means of achieving this would employ two or more gratings mounted on a common shaft, the angular position being set by a small torque motor.

To illustrate this, we consider the far ultraviolet region accessible with lithium fluoride optics and a CsI photocathode, roughly 1150 - 1900 A. The spectral characteristics for 0.1 mm detector elements in the direction of the dispersion are given in Table I for three different grating rulings. The practical limit, in this case using the gratings in

first order to avoid overlapping orders and order sorting filters (which are very inefficient in the far ultraviolet) is about 0.5 A. The most useful case, for atmospheric spectroscopy, where a resolution of 10 A is often more than adequate is provided by the 980 ℓ/mm grating which would cover 500 A at one time and require only 2 grating positions to allow complete coverage of the spectral range. A list of other spectral properties for other visible and near ultraviolet sensitive detectors is given in Table II.

E. Sensitivity

The principal advantage of the multi-element detector array arises from the fact that each spectral and spatial element is observed for the full time of the observation, and that all spectral elements are observed simultaneously so that time histories of different emission lines can be obtained with a single instrument. This latter case is especially useful in determining delay times in the emission of radiation from metastable atomic or molecular states relative to the prompt emission coincident with a given excitation process. In the one-dimensional case, if we have N spectral elements and the observing time is T, for a scanning spectrometer each element would be observed for a time T/N, as opposed to time T for the multi-element detector, so that in the case where the counting statistics determine the sensitivity limit, the signal-to-noise improvement for the multi-element detector is $N^{1/2}$. For 256 elements this improvement is 16. Note, however, that in order to achieve this with a scanning spectrometer an increase in observing time of a factor N would be required. This advantage has been recently achieved in a rocket-borne spectrometer

Table I

Grating (ℓ/mm)	980	3600	5670
Dispersion (A/mm)	20	5	3
Wavelength Span in 25 mm (A)	500	125	75
Number of Detector Elements	250	250	250
Resolution Element (A)	2	0.5	0.3
Number of grating positions to cover entire range	2	6	10

Table II

Spectral Range	1800-3000 A	3000-6000 A
Photocathode	RbTe	Bi-alkali
Grating (ℓ/mm)	980	300
Dispersion (A/mm)	20	64
Wavelength Span in 25 mm (A)	500	1600
Resolution Element (A)	2	6.4

used by Vitz et al. (1976) to observe stars in the far ultraviolet. An improvement in signal/noise ratio of ≈8, nearly the theoretical value, was achieved with a 100 element detector over a previous measurement with a scanning instrument (McKinney et al., 1976).

For a diffuse radiation source of brightness B_s expressed in Rayleighs, the signal in counts sec^{-1} can be written as

$$S_\lambda = B_s \cdot \frac{10^6}{4\pi} \cdot \frac{A_s A_g Q_\lambda T_\lambda \cos \alpha}{F^2} \qquad (11)$$

where A_s is the element of slit area imaged onto

a detector element, in our case $\Delta x \Delta y$,

A_g is the ruled area of the grating,

Q_λ is the detector quantum efficiency at wavelength λ,

and T_λ is the spectrometer transmission at λ. Generally, the calibration technique will measure the product $Q_\lambda T_\lambda$ (see Appendix B). In terms of the dispersion and the spectral and spatial resolution elements we have

$$A_s = \Delta x \Delta y = \Delta\lambda \Delta z_e D_\lambda^{-1} D_z^{-1} \qquad (12)$$

Defining S_λ as the sensitivity in photoelectrons sec^{-1} R^{-1} we can rewrite Eq. 11 as

$$S_\lambda = \left(\frac{10^6}{4\pi} \cdot \frac{A_g}{F^2}\right) (Q_\lambda T_\lambda \cos \alpha) (\Delta\lambda \Delta z_e D_\lambda^{-1} D_z^{-1}) \qquad (13)$$

where the first term on the right contains only the spectrometer dimensions, the second term is wavelength dependent and the third term depends on the choice of spectral and spatial resolution and dispersion. If the instrumental resolution is greater than the $\Delta\lambda$ corresponding to

a single detector element, then by summing all of the elements in an instrumental half-width we get the resultant sensitivity which is equivalent to using the FWHM for $\Delta\lambda$ rather than the detector element. An example of S_λ obtainable with the instrument described in Table I is given in Table III, where the element of height resolution has been taken to be 0.5 mm in the focal plane. This corresponds to $\Delta z_e \approx 1$ km for a 0.5 m focal length telescope.

Increased sensitivity can be achieved at a loss of spatial information by orienting the spectrometer entrance slit parallel to the horizon as shown in Fig. 1c. In this case the telescope images a horizontal slice of the limb of height Δz_e onto the entrance slit and all of the detector elements at a given wavelength receive radiation from the same height region of the atmosphere. In terms of the entrance slit spectral width $\delta\lambda$, this height element is given by

$$\Delta z_e = \delta\lambda \cdot D_\lambda^{-1} \cdot D_z \tag{14}$$

and for a slit of length $\underline{\ell}$, the sensitivity S'_λ obtained by summing the counts from all of the vertical detector elements is then

$$S'_\lambda = \left(\frac{10^6}{4\pi}\,\frac{A_g}{F^2}\right)\,(Q_\lambda\, T_\lambda \cos\alpha)\,\left(\ell\,\Delta\lambda \cdot D_\lambda^{-1}\right) \tag{15}$$

Examples of obtainable S'_λ are also given in Table III, and it can be seen that emission features of the order of 3 Rayleighs can be detected at 10 A resolution in 1 second with approximately 10% statistical uncertainty.

Table III

Spectrometer Sensitivity

Focal Length	0.5 m	
Grating	3600 ℓ/mm	980 ℓ/mm
A. Slit Vertical		
Spectral Resolution, $\Delta\lambda$	10 A	10 A
Spectral Dispersion, D_λ	50 A/cm	196 A/cm
Spatial Resolution, Δz_e	1 km	1 km
Grating Area, A_g	10^2 cm^2	10^2cm^2
Satellite Altitude, z_o	250 km	250 km
Viewing Altitude, z_e	100 km	100 km
Spatial Dispersion, D_z	28 km/cm	28 km/cm
$Q_\lambda T_\lambda$ (mean 1200-1500 A)	0.02	0.02
S_λ (per height element)	0.45 pe sec^{-1}R^{-1}	0.12 pe sec^{-1}R^{-1}
B. Slit Horizontal		
Spectral Resolution, $\Delta\lambda$	10 A	10 A
Height Element, Δz_e	5.6 km	1.4 km
Slit Length, ℓ	2.5 cm	2.5 cm
S'_λ	32 pe sec^{-1}R^{-1}	8 pe sec^{-1}R^{-1}

Note that S'_λ also describes the sensitivity of the spectrometer when used without the fore-optical telescope. In this case, S'_λ refers to the average brightness in a field roughly 10 x 12°.

F. The Extreme Ultraviolet

Below 1100 A, the reflectivity of overcoated aluminum surfaces decreases rapidly and the efficiency of the Ebert mount, which requires three reflections, becomes very poor. For this region a more suitable spectrometer configuration is the Paschen mount in which a concave grating is used together with an entrance slit and detector array located on the Rowland circle, as shown in Fig. 4. Suitable materials for overcoating the grating exist which provide reflectivities at near normal incidence of 10-20% or greater for all wavelengths above 300 A, which is the lower end of the range of interest in atmospheric spectroscopy. The only aberration to consider is astigmatism which is described by Eqs. 7 and 8 with a_1 replaced by α, the angle between the central incident ray and the grating normal. For a 0.5 m spectrograph with a 3600 ℓ/mm grating operating between 500 and 900 A, $\Delta\ell' \approx 0.5$ mm for an f/10 system. The concave grating instrument will thus have the same height resolution as the f/5 Ebert spectrometer described above but it will be a slower instrument.

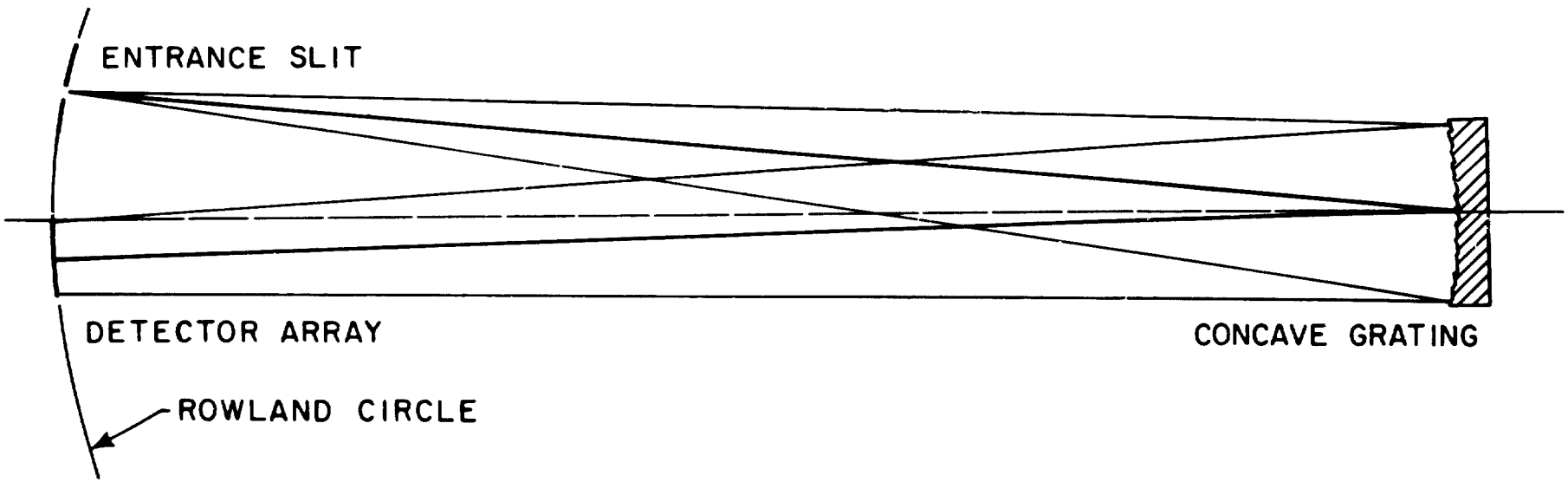

Fig. 4. Concave grating spectrometer for the extreme ultraviolet

III. Detector Arrays

Imaging photoelectric detectors exist today in several different forms. For the visible, near-ultraviolet and near-infrared there are large families of vidicons and image orthicons which can provide large image area (the 25 x 25 mm^2 size used in the spectrometer calculation is by no means the largest available) and high resolution ($\approx$ 0.025 mm). In these devices, photoelectrons produced at the photocathode are accelerated and magnetically or electrostatically focussed onto a target in which charge multiplication occurs. Charge stored in the target is then read out using a raster scanning electron gun. Another type of charge storage detector, a more recent semiconductor development, is the charge-coupled device (CCD), and in this case the optical image is formed directly on the device. A review of the state-of-the-art (as of 1972) of these types of devices is available as a report of a NASA symposium (Sobieski and Wampler, 1973).

For the vacuum ultraviolet, these detectors would have to be used with an image converter, which in addition to increasing the size and complexity would tend to degrade the sensitivity and resolution of the detector. Furthermore, the sensitivity of a vidicon type detector is limited at very low light levels by preamplifier noise since the read-out system is basically an analog measurement. The dynamic range is also limited by the spreading of charge within the target material. These two properties are exactly the opposite of what is desired in a detector for atmospheric spectroscopy.

A more attractive detector for the vacuum ultraviolet is the micro-channel plate (MCP) detector, shown in Fig. 5, which is an array of glass channel electron multipliers, each acting as an independent photomultiplier. If an image is formed on the input side of the MCP, the emerging multiplied electron pulses will retain the image properties to a resolution equal to the spacing between adjacent channels which is typically of the order of .02-.05 mm. In the ultraviolet, with either a coated or uncoated input surface, the MCP has virtually no dark count rate, so that it would appear to have the ideal properties for an image retaining pulse counting detector. The problem in using the MCP is to find the means to record the arrival of a pulse as well as its position, in two dimensions, relative to some fiducial axis on the array. An obvious technique is to use the MCP as an image converter in which the output electron pulses produce a visible image on a phosphor screen which is then recorded by a vidicon-type device. However, this would negate the advantages gained by pulse counting and is not desirable.

In practice, the MCP is hardly an ideal pulse counting detector. A single channel in a MCP does not behave like a channel electron multiplier because ion feedback in the straight channel limits the maximum gain to less than 10^4 and the resultant pulse height distribution is a gradual exponential. To reduce the ion feedback and increase the gain to where a saturated pulse height distribution is obtained, two MCPs

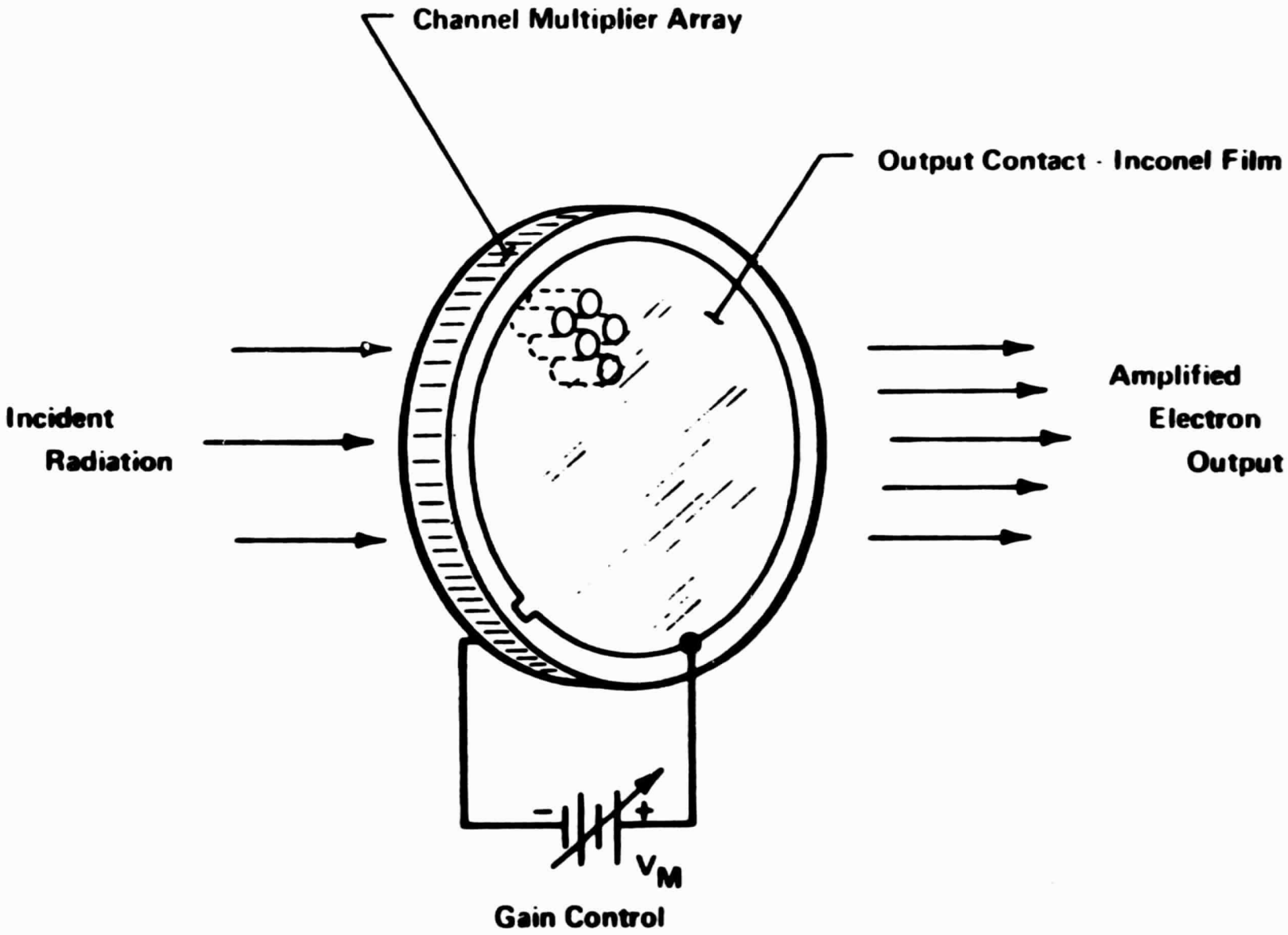

Fig. 5. Micro-channel plate detector. From D. J. Ruggieri, IEEE Trans. Nuc. Sci., Vol. NS-19, No. 3, June 1972.

are used in the chevron arrangement shown in Fig. 6. Pulses of 10^7 electrons or greater can then be detected by a suitable device mounted in close proximity to the near MCP surface.

In the last few years, several techniques for direct readout of micro-channel plate arrays have been developed for use in ultraviolet and soft x-ray astronomy. One-dimensional detectors have recently flown successfully on several rocket experiments and prototype detectors are being tested for Mariner/Jupiter/Saturn and High Energy Astrophysical Observatory-B. The techniques fall into two general categories; those that use division of charge to compute the pulse position, such as the resistive anode (Lampton and Paresce, 1974; Lawrence and Stone, 1975), and those that use discrete charge collection, such as the Digicon (Tull et al., 1975) or the multianode detector (Timothy and Bybee, 1975, 1976). An interesting hybrid is the cross-grid readout of Kellogg et al. (1976) being developed for HEAO-B.

Resistive anodes, which employ charge division, are basically simpler devices requiring either 2 or 4 preamplifiers for a 1 or 2 dimensional readout, respectively. However, the analog calculation of pulse position is time consuming and a practical upper limit of 2×10^4 counts sec^{-1} (over the entire area of the detector) has been obtained. A comprehensive survey of charge division techniques and various electronic readout schemes is given by Lampton and Paresce (1974). The relatively low dynamic range resulting from the low maximum counting rate

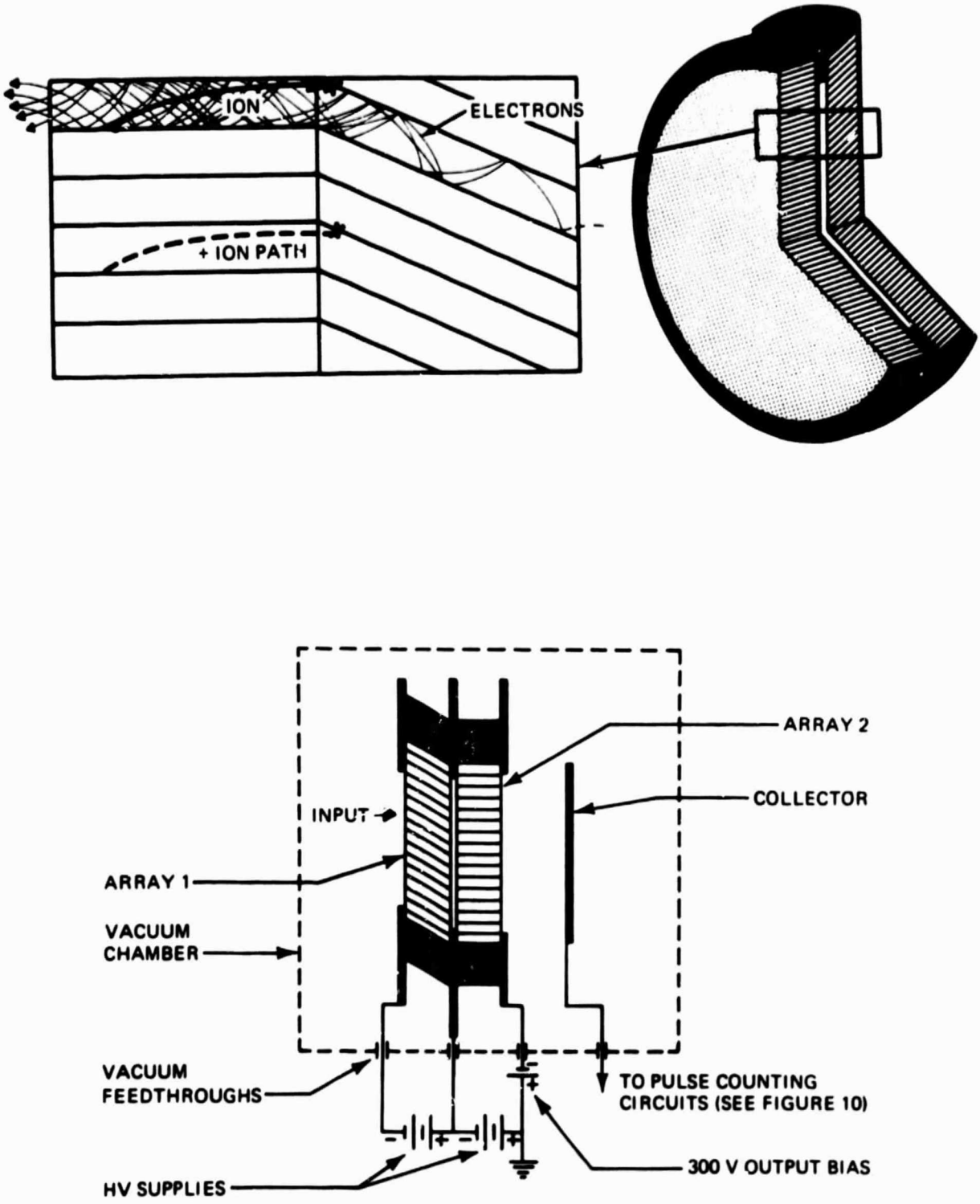

Fig. 6. Micro-channel plate chevron arrangement for pulse counting. From Bendix Technical Application Note on the Bendix Chevron Channel Electron Multiplier Array.

is not often a serious problem since in general a multi-element detector will be employed mainly in the observation of weak sources. However, when calibration using bright sources is necessary or when a larger dynamic range is needed to avoid saturating a detector on strong signals which would tend to prevent the detection of the weaker features, some other means must be found to reduce the count rate. Both Vitz et al. (1976) and Lawrence and Stone (1975) have successfully flown one-dimensional resistive strip detectors on Aerobee rockets achieving a resolution of 0.1 mm, and a two-dimensional "Ranicon" (Lampton and Paresce, 1974) will be flown this year.

Of the discrete detector systems, the Digicon (Tull et al., 1975) uses a self-scanning diode array, which like the Vidicon is an analog system. For MJS, electrons from the MCP will strike the diodes directly, unlike previous systems in which the MCP and diode array were used as an image converter. In the self-scanning mode, only one amplifier is needed since the diodes are sampled in succession and the total charge accumulated since the previous readout is determined as an analog voltage. This device is particularly useful in ground-based astronomical spectroscopy in the visible region of the spectrum as described by Tull et al. (1975). Timothy and Bybee (1975, 1976) have described both one- and two-dimensional array detectors (Fig. 7) in which individual pulses are collected by evaporated wires connected to individual preamplifiers. For an array of N wires, N amplifiers are

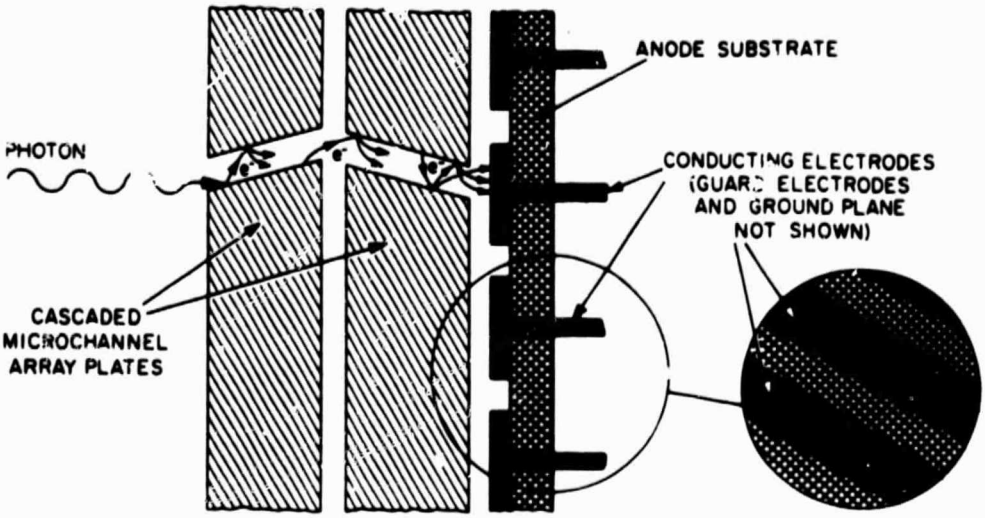

PROXIMITY - FOCUSED
DISCRETE - ANODE ARRAY

(a)

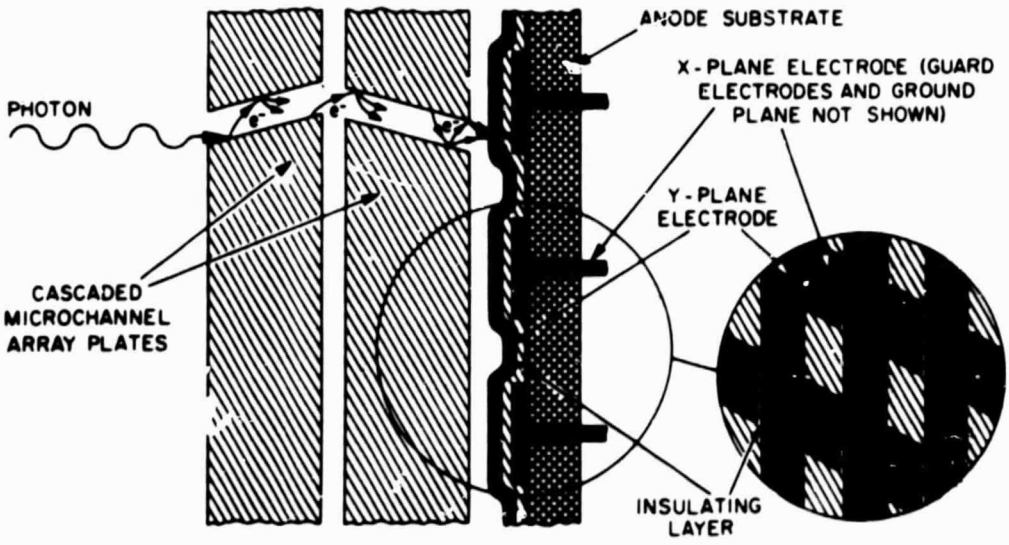

PROXIMITY - FOCUSED
DISCRETE - ANODE COINCIDENCE
ARRAY

(b)

Fig. 7. Discrete anode array detectors.
From Timothy and Bybee (1976)

needed. The two-dimensional version employs crossed arrays and coincidence circuitry to identify the two orthogonal coordinates of a given pulse. For an array of N x M detector elements, N + M pre-amplifiers are necessary. In the previous section we used a 250 x 50 array which would necessitate 300 separate high input impedance amplifier circuits, which even with current microelectronics capability would lead to large volume and power requirements and reliability problems. However, the system is the fastest of any considered with counting rates in excess of 10^6 counts sec^{-1} possible. The ultimate limit will probably be set by the maximum rate at which a microprocessor can handle the position information. Also, this system is perhaps the most flexible for atmospheric spectroscopy in being able to exclude unwanted data, vary the basic detector element size or achieve high temporal resolution.

The crossed-grid readout of Kellogg et al. (1976) also uses crossed arrays of wire detectors, but these are self-suspended rather than deposited on a semiconductor substrate as are those of Timothy and Bybee (1976). Each set of eight wires is resistively coupled to a single amplifier so that charge division is used over a relatively small range. In devices built to date, a resolution of 0.02 mm has been achieved with wires spaced 0.2 mm apart (and amplifiers 1.6 mm apart). For a 25 x 25 mm array 32 separate amplifiers are needed. The decoding logic for this system is perhaps the most complex of any system currently in

use, although the 10 times reduction in the number of amplifiers over the Timothy and Bybee readout is a clear advantage. It should be noted that all of the discrete readout systems have been built on a relatively small scale and that a full array for a 25 x 25 mm^2 detector does not exist at present.

Finally, we wish to comment that the foregoing discussion points up the need, regardless of which system is used, for a dedicated microprocessor/computer to control the spectrometer and accumulate, store, process and transmit the data from the multi-element detector. A minimum core size, for data storage alone, is N x M which is of the order of 10^4 for a 250 x 50 element array.

IV. Conclusion

In the preceding discussion, the optical properties of a multi-element detector spectrometer have been evaluated for an instrument of the size and weight suitable for inclusion in the AMPS payloads aboard Spacelab. Within this constraint, it is found that spectrometer designs of the type currently used in various space applications, can be used with sufficient spectral and spatial resolution to satisfy the requirements for atmospheric spectroscopy and with a substantial improvement in sensitivity over scanning instruments. For the vacuum ultraviolet, the microchannel plate array detector allows for pulse-counting detection of individual photoelectrons while at the same time not impairing the

system resolution set by the optics. The major problem is detector readout and the development of several different techniques is currently in progress for various NASA programs such as Large Space Telescope, Mariner Jupiter/Saturn and HEAO-B. The choice for the AMPS spectrometers will depend on the ability of a given system to provide the flexibility and time resolution required for the different types of atmospheric experiments to be flown on AMPS. Similar spectrometers and detector systems can be used in the visible and near-infrared regions of the spectrum by using the MCP detector in a sealed tube behind a suitable semi-transparent photocathode, so that an array of similar spectrometers and ancillary electronics can be used to span the entire spectral region from vacuum ultraviolet to near-infrared and since the instruments are similar the design and fabrication costs can be minimized. An instrument description of such a candidate array for AMPS is given in Appendix A.

Besides the problem of detector readout, another problem arises from the implicit nature of multi-element detectors, namely the large volume of data that must be processed. In a space laboratory with many instruments operating simultaneously, telemetry bandwidth available to a single experiment is limited, and even if all of the raw data could be transmitted to the ground, much of it would often be unneeded. Thus, any readout system must be coupled with a dedicated microprocessor which, in addition to controlling the instrument and collecting

the data, would also be able to interact with the experimenter to determine how to select the data and choose the proper format for transmission. The interface between this microprocessor and the Spacelab computer is thus vital to the successful operation of a multi-element detector spectrometer on AMPS.

Finally, one problem area which has not been discussed above is that of photometric calibration of detector arrays and in particular the variation in effective quantum efficiency with position on the array. In recent years there have been considerable advances in calibration techniques for the vacuum ultraviolet. In Appendix B, we include a description of the facility which was built at Johns Hopkins University for the calibration of the Apollo 17 Far Ultraviolet Spectrometer and which appears ideally suited for the calibration of multi-element detector spectrometers.

References

Fastie, W. G., Image forming properties of the Ebert monochromator, J. Opt. Soc. Am. 42, 647, 1952.

Fastie, W. G., H. M. Crosswhite and D. F. Heath, Rocket spectrophotometer airglow measurements in the far ultraviolet, J. Geophys. Res. 69, 4129, 1964.

Henry, R. C., A. Weinstein, P. D. Feldman, W. G. Fastie and H. W. Moos, Low-resolution ultraviolet spectroscopy of several hot stars observed from Apollo 17, Astrophys. J. 201, 613, 1975.

Kellogg, E., P. Henry, S. Murray, L. Van Speybroeck and P. Bjorkholm, High resolution imaging x-ray detector, Rev. Sci. Inst., in press, 1976.

Lampton, M. and F. Paresce, The Ranicon, A resistive anode image converter, Rev. Sci. Inst. 45, 1098, 1974.

Lawrence, G. M. and E. J. Stone, Ultraviolet spectrograph using microchannel plate, Rev. Sci. Inst. 46, 432, 1975.

McKinney, W. R., H. W. Moos and J. W. Giles, The far ultraviolet (1180 A-1950 A) emission spectrum of Arcturus, Astrophys. J., in press, 1976.

Shafer, A. B., L. R. Megill and L. Droppleman, Optimization of the Czerny-Turner spectrometer, J. Opt. Soc. Am. 54, 879, 1963.

Sobieski, S. and E. J. Wampler, Eds., Advanced Electro-Optical Imaging Techniques, NASA SP-338, 1973.

Strong, J., Concepts of Classical Optics, W. H. Freeman and Co., San Francisco, 1958.

Timothy, J. G. and R. L. Bybee, One-dimensional photon-counting detector array for use at EUV and soft x-ray wavelengths, Appl. Opt. 14, 1632, 1975.

Timothy, J. G. and R. L. Bybee, Two-dimensional photon-counting detector arrays based on microchannel array plate, Rev. Sci. Inst., in press, 1976.

Tull, R. G., J. P. Choisser and E. H. Snow, Self-scanned Digicon: a digital image tube for astronomical spectroscopy, Appl. Opt. 14, 1182, 1975.

Vitz, R. C., H. Weiser, H. W. Moos, A. Weinstein and E. S. Warden, Spectroscopic survey of the far ultraviolet (1160-1700 A) emissions of Capella, Astrophys. J. (Letters), in press, 1976.

APPENDIX A

Instrument Description for AMPS Instrument No. 3,

Multiple Spectrometers, October 10, 1975.

INSTRUMENT NO. : 3

I. Title: MULTIPLE SPECTROMETERS

II. Objective: Monitoring of atmospheric emissions in the spectral range of 300 to 8,000 A. These emissions will be both naturally occurring solar-induced emissions and emissions resulting from simulation experiments conducted aboard Spacelab such as electron beam injection and chemical releases.

III. General Description:

A. Configuration: The entire spectral range is covered by a series of four spectrophotometers, each optimized by choice of grating ruling and photocathode to provide maximum sensitivity in about one octave of the spectrum. The use of two-dimensional multi-element photon counting detector arrays will simultaneously provide spectral resolution and one-dimensional spatial resolution when the spectrometers are used with an auxiliary telescope. Both high and low resolution will be available via interchangeable gratings. High sensitivity can be achieved at a loss of spatial resolution by simply rotating the spectrometer by 90^{o} in a limb-viewing geometry. In this case the feature of being able to observe several emission lines simultaneously is maintained. The basic configuration of the spectrometer array would consist of four spectrometers for the following bands:

300 - 1100 A (extreme ultraviolet)

1100 - 1900 A (far ultraviolet)

1900 - 4000 A (near ultraviolet)

4000 - 8000 A (visible-near infrared)

The extreme ultraviolet spectrometer would be a concave grating instrument while the other three would be of the Ebert-Fastie design. The focal length of all spectrometers will be 0.5 m.

B. Subsystems:

1. Telescope and deployment mechanism
2. Entrance slit width mechanism
3. Grating position mechanism
4. Multi-element detector system and electronics (most likely a dedicated microprocessor)

C. Specifications:

Spectral Characteristics:

Spectral Range: See III. A above

Spectral Resolution: Depends on grating ruling and entrance slit width, but typically it will be possible to go from 0.5 A to > 10 A in the ultraviolet. The spectral resolution $\Delta\lambda$ is related to the spectral range covered by a given grating $(\lambda_2 - \lambda_1)$ by

$$\frac{\Delta\lambda}{\lambda_2 - \lambda_1} = \frac{1}{N_d}$$

where N_d is the number of detector elements in the direction of the dispersion. For a 0.5 m focal length spectrometer with a 25 x 25 mm^2 detector, aberrations limit N_d to $\approx$ 250.

Sensitivity: The signal, S, in photoelectrons sec^{-1} $Rayleigh^{-1}$ for the spectrometer just described in a limb viewing mode (slit perpendicular to horizon) is given by:

$$S_\lambda = 3.2 \times 10^3 \, QT \, \Delta z \, \Delta\lambda \, D_z^{-1} \, D_\lambda^{-1}$$

where Q = quantum efficiency of the detector at wavelength λ

T = transmission of spectrometer and telescope at λ

Δz = element of height resolution in km

$\Delta\lambda$ = element of spectral resolution in A

D_z = spatial dispersion in km cm^{-1}

D_λ = spectral dispersion in A cm^{-1}.

For an example we take a spectrometer flying at 250 km altitude, with a grating of 980 l/mm, near 1400 A the sensitivity for 10 A spectral resolution, 1.2 km spatial resolution is 0.13 pe $sec^{-1} R^{-1}$.

Viewing with the slit parallel to the horizon the sensitivity is increased to

$$S_\lambda' = 8.0 \times 10^3 \, QT \, \Delta\lambda \, D_\lambda^{-1}$$

where now $$\Delta z = \Delta\lambda \cdot \frac{D_z}{D_\lambda}$$

In the above example $S_\lambda' = 8.0$ pe $sec^{-1} R^{-1}$.

The minimum detectable signal will ultimately be determined by the detector dark count rate and the scattered light signal.

Field of View: $12^{o} \times 10^{o}$ without telescope (except for the EUV spectrometer which is $\sim 5^{o} \times 5^{o}$). $2.9^{o} \times (0.01^{o}$ to 0.1^{o} depending on entrance slit width) with telescope.

Dynamic Range: At least 10^{4} photoelectrons sec^{-1}.

Spatial Resolution: $\approx$ 1 km in limb viewing geometry.

Off-Axis Rejection: System must be baffled from sunlight to permit daytime observations to within 30^{o} of the sun.

Time Constant: Data is processed in real-time by dedicated microprocessor. Readout time is determined by rate at which data can be read from microprocessor memory. Accumulation time is controlled by the experimenter and can range from a practical minimum of $\approx$ 0.1 sec to several hours.

Accuracy: Photometric calibration of all of the spectrometers will be better than 20%. Inflight calibration using stellar sources will be used to monitor possible instrument degradation.

Polarization: TBD

Detector: Multielement array consisting of a pair of microchannel plate detectors and a suitable readout device still to be determined. The detectors for wavelengths longer than 2000 A will be sealed units. For the vacuum ultraviolet instruments the detectors will be windowless but will require being kept under vacuum before launch in order to prevent deterioration of the photocathode surface.

Power: Mechanical subsystems: Intermittent use ~ 10 W. Each detector: TBD (depends on detector readout device and microprocessor)

Physical Dimension and Weight:

Each Spectrometer (including detector): 0.3 m x 0.3 m x 1 m.

Telescope: TBD, depends on baffling.

Weight: 15-20 kg total for each spectrometer.

IV. Operation:

A. Pointing Requirement: ~ 6 arc minutes.

B. Spacelab position and altitude: $\geq$ 250 km. Spectrometer must be able to view towards limb, zenith or nadir. Slit orientation must be variable.

C. Stabilization: $\leq$ 1 arc minute in limb viewing mode.

D. Frequency and duration of data taking: See Time Constant section.

E. Cooling: Ordinary ventilation for the electronic equipment.

F. Complementary operation: TBD.

V. Checkout and Test:

A. Boresighting Requirement: TBD

B. Prelaunch Checkout: Normal functional checks.

C. Prelaunch Calibration: Calibrations at the lab before delivery is adequate.

D. Inflight Calibration: Inflight calibration using stellar sources will be used to monitor instrument status and provide an inflight photometric calibration.

VI. Control and Display:

A. Control: The following control functions should be provided for each instrument:

Power (On/Off)

Select Telescope (yes or no)

Select Slit Orientation

Select Wavelength Range

Select Dispersion

Select Accumulation Time and Readout Time

B. Display: The following displays are required for each instrument:

Two-dimensional raster (counts vs. z and λ)

One-dimensional plot of a) counts vs. z (constant λ)

b) counts vs. λ (constant z)

VII. Data:

A. Scientific: Bit rate depends on readout rate from microprocessor memory. For example, a 50 x 250 element array will require 1.25×10^4 storage locations. If each word is 8 bits, then the total data requirement is 10^5 bits, or a 10^5 Hz bit rate for a 1 sec readout. However, it should be possible to program the readout of only a small part of the memory at a higher sample rate (bit rate remaining constant) depending on the requirements of the experimenter.

B. Housekeeping: 3 analog channels per spectrometer.

VIII. Development Status: The only area in need of development is that of detector readout and associated microprocessor.

APPENDIX B

Spectroradiometric Calibration Techniques in the Far Ultraviolet: A Stable Emission Source for the Lyman Bands of Molecular Hydrogen, by W. G. Fastie and Donald E. Kerr. Appl. Opt. 14, 2133, 1975.

Reprinted from APPLIED OPTICS, Vol. 14, page 2133, September 1975

Spectroradiometric calibration techniques in the far ultraviolet: a stable emission source for the Lyman bands of molecular hydrogen

W. G. Fastie and Donald E. Kerr

The problems associated with making accurate spectroradiometric measurements in the far uv region are sketched briefly. The equipment and methods that were developed for providing absolute sensitivity calibration of an Apollo 17 far uv spectrometer are described. The absolute reference standards were photoelectric diodes calibrated at the National Bureau of Standards. A complete vacuum optical facility, which included a premonochromator and stable uv light sources, was developed to calibrate the Apollo 17 instrument, and it has been used for a number of other tasks. Absolute radiometric calibrations between about 1200 Å and 1700 Å were performed with an absolute accuracy of ±10%. The light source, which was designed to provide a very stable light output, is a low-pressure molecular hydrogen lamp in which the pressure is stabilized by thermal control of uranium hydride powder. Individual emission lines of the Lyman molecular band system of H_2 are used for calibration purposes. The lamp also copiously emits the 1215.7 Å line (Lyα) of atomic hydrogen.

I. Introduction

There is increasing demand in laboratory and space physics for accurate measurement of spectral radiance of many kinds of light sources in the vacuum uv region. This paper describes some techniques and equipment that were developed initially for absolute calibration of the Johns Hopkins University uv spectrometer on the Apollo 17 mission.[1,2] With small modifications, however, they have been directly applicable to numerous other rocket and satellite spectrometers in the 115–3000-Å wavelength range.

A major difficulty in this field is that there is no reasonably simple primary standard source of spectral radiance in the vacuum uv region. Although good progress has been made in applying the wall-stabilized hydrogen arc to this purpose,[3] the arc is not yet ready for the present task. The alternate route of applying various forms of absolute or transfer standard detectors is equally useful for many purposes. A good review of the latter possibilities has been given by Canfield *et al.*[4]; they outline the major reasons that make the transfer standard detector particularly useful for the needs of our program. Vacuum photodiodes of good stability are now available commercially, and the National Bureau of Standards can provide absolute calibrations of their sensitivity to an accuracy believed to be[4] within ±6%. Other developments described here, including stable uv light sources, vacuum optical facilities of moderate size, and methods of measuring polarization and scattered light produced by optical components, have aided greatly in simplifying the calibration problem. By appropriate combinations of these techniques we believe that we can now consistently obtain absolute calibrations of instrument sensitivity to within ±10%, including the uncertainty for the photodiode.

When this work was done, both authors were with The Johns Hopkins University, Physics Department, Baltimore, Maryland 21218. D. E. Kerr died 20 May 1975.

Received 19 March 1975.

II. General Description of Method

A diagram of the calibration system is shown in Fig. 1. Light from the uv source (a stable discharge tube) is passed through a premonochromator with a small exit slit to a concave transfer mirror M_T, which can be rastered in two dimensions so that the entire image of the premonochromator exit slit can be directed to all points within the entrance slit of the spectrometer to be calibrated. The premonochromator has sufficient resolution to isolate individual emission lines of a gaseous discharge source. Alternatively, the beam can be offset to illuminate about a 1-cm² area of either of two reference photomultiplier tubes, which are between the mirror and the spectrometer. A mask at the plane folding mirror M_F limits the relative aperture of the beam to $f/80$. The reference photomultiplier tubes to which the premonochromator beam can be directed are calibrated be-

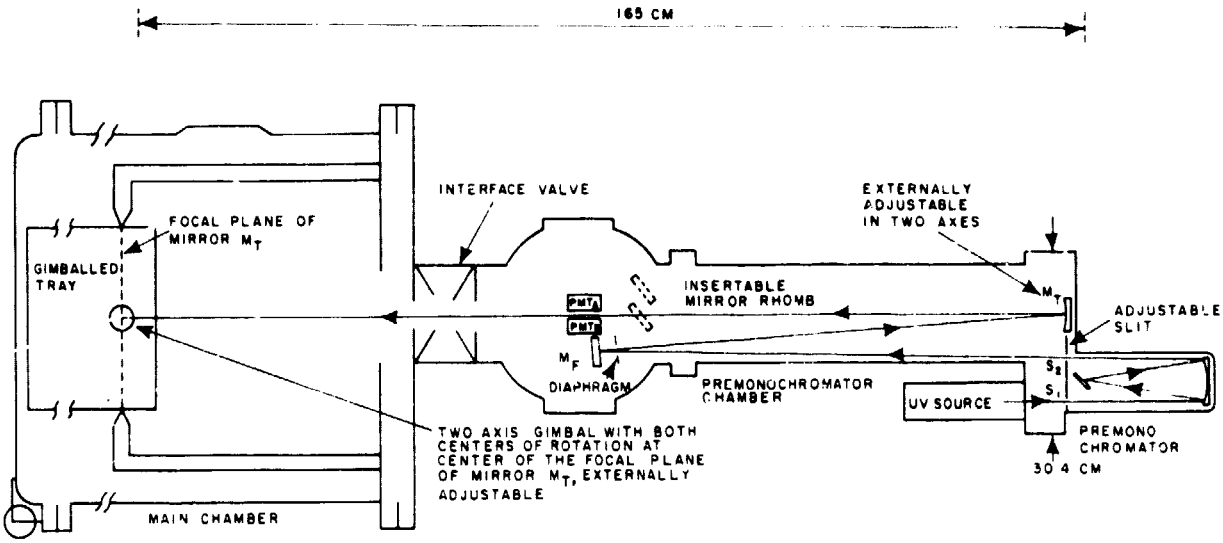

Fig. 1. Schematic diagram of calibration test equipment (plan view).

fore and after the spectrometer is installed by placing a diode, calibrated at the National Bureau of Standards, at the spectrometer location so that the photon flux in the beam can be determined at all wavelengths of interest. The spectrometer is mounted in the vacuum chamber on a gimballed plate, which is so arranged that the centers of rotation of the two axes coincide with the center of the entrance slit and with the center of the focal plane of the transfer mirror M_T. Two-axis motion of the gimballed plate provides the means to direct the narrow calibrated beam to any area of the dispersing element.

The calibration measurements provide a determination of the product of the optical transmission of the spectrometer and the electronic conversion efficiency of the detector over the aperture of the spectrometer, over the pertinent area of the entrance slit, and over the wavelength range of interest. That is, the output signal S_0 in whatever units it represents is related to the input signal S_λ in photons by the relationship

$$S_0 = S_\lambda K_\lambda, \tag{1}$$

where K_λ is proportional to the product of the optical transmission and the electronic conversion efficiency. K_λ is a constant for each wavelength if the detector and subsequent electronic circuits are linear over the required dynamic range of the instrument. Photomultiplier tubes are linear over about 5–6 orders of magnitude when used in the current mode, but wide-range linear subpicoampere to microampere electrometers tax the state of the art; thus calibration at different signal levels is necessary if the full dynamic range capability of PM tubes is to be employed. Photoelectron-counting circuits do not normally have a wide dynamic range or may be purposely designed to be nonlinear for purposes of data compression. In any case, by varying S_λ during the testing over the dynamic range in which the spectrometer is to be used provides a means of determining the variation of K_λ with light intensity.

There are often several modes of operation for the calibrated instrument, and each mode uses different geometrical and observational parameters to determine the absolute brightness of the observed radiating source. For example, if no external optics are used and the instrument observes an extended monochromatic source that fills the optical aperture, the radiance of the source B in photons/sec/cm^2/sr is given by

$$B = \frac{S_0 F^2}{K_\lambda A_s A_g}, \tag{2}$$

where F is the focal length of the spectrometer collimator;
A_s is the area of the entrance slit; and
A_g is the projected area of the dispersing element.

If an extended source has a uniform spectral continuum of spectral radiance B_λ in photons/sec/cm^2/sr/Å, the spectral width $\Delta\lambda$ of the exit slit must also be known and

$$B_\lambda = \frac{S_0 F^2}{K_\lambda A_s A_g \Delta\lambda}. \tag{3}$$

Note that the length of the exit slit is not a parameter because the calibration procedures described below have indirectly included it.

If the spectrometer is employed without external optics to measure the absolute flux F_λ from a distant point source (a star) with a uniform spectral continuum

$$F_\lambda = \frac{S_0}{A_s K_\lambda' \Delta\lambda} \text{ (photons/sec/cm}^2\text{/Å)}, \tag{4}$$

where K_λ' is the calibration constant applicable to the restricted area of the dispersing element which is illuminated.

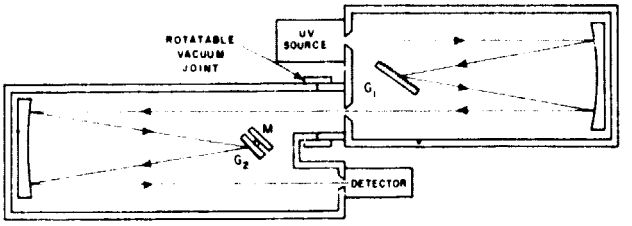

Fig. 2. Vacuum double monochromator with 90° rotation capability between first and second monochromator.

If external reflecting optics are employed to focus an image of a distant source onto the spectrometer entrance slit, it is necessary to know the transmission coefficient of the telescope over the applicable wavelength range. It is often adequate to use test samples in association with the reflecting elements when they are coated to determine the transmission coefficient of the external optical system. Alternatively, the transmission of the telescope system can be measured or the system can be attached to the spectrometer and an over all calibration obtained. We usually employ the latter methods for purposes of obtaining a cross check on the absolute accuracy. For these purposes we replace the folding mirror in the calibrated beam (Fig. 1) with a convex mirror to produce a parallel beam that is focused by the external optics of the spectrometer onto the entrance slit. The parallel beam is narrow enough so that all the photons in the beam can be intercepted by the reference photomultiplier tubes and by the calibrated diodes.

III. Polarization Studies

To establish that the gratings in monochromators that we have employed for our rocket and satellite experiments do not introduce significant polarization we have employed a double vacuum monochromator with a flight prototype grating in the first monochromator and the other with an identical grating, both being replicas from the same master grating.

The experimental equipment for investigating polarization effects is shown in Fig. 2. Light from a stable far-uv light source is sent through a first vacuum monochromator and then through a second monochromator to a stable photomultiplier tube detector. The mechanical interface between the two monochromators includes a tubular section that permits the second monochromator to be rotated about an axis that is coincident with the central ray of its entrance beam. The vacuum pumping system is attached to a pumping port on the first monochromator and also to a pumping port on the fixed section of the interface tube between the two monochromators. The mirror M in the second monochromator can be substituted for the grating G_2 so that the grating G_1 can be tuned to the peak signal from an emission line of the source. Then the second grating is rotated to the desired grating order, and the detector signal is measured. Next the entire second monochromator is rotated through an angle of 90° about the common axis, and the detector signal is again measured. The ratio of signals from the two positions can be measured to about 1% or 2%, and to within this uncertainty we have not been able to detect any polarization in replica gratings of 3600 g/mm in the 1200–1800-Å range with replicas made from several Bausch & Lomb masters.

IV. Component Evaluation

The equipment shown in Fig. 2 can be used for additional measurements. If the reflectivity of the mirror M is known, the absolute efficiency of the grating G_2 can be determined at any wavelength by measuring the ratio of the detector signal produced by the grating to that from the mirror. Likewise the scattering properties of the grating G_2 can be determined by setting the first monochromator on a bright spectral feature and measuring the detector signal from that spectral feature and the signals obtained for all angular positions of the grating G_2. For most accurate measurements of scattered light it is desirable that the uv source be monochromatic or that only its strongest spectral features be employed so that the effect of light scattered by the first monochromator is minimized.

Figure 3 shows information obtained in the CTE on scattering of light by gratings. The center of the Apollo flight grating was illuminated with Lyman α radiation. The scattered light reveals at least two families of Rowland ghosts plus a scattering continuum that apparently originates at the grating. This type of laboratory data has proven invaluable in the search for weak emissions from the various objects that were studied during the mission.

We have also used this test equipment to compare detector systems for flight packages with calibrated laboratory detectors and with diodes calibrated at the National Bureau of Standards. Similarly, we have tested mirrors for flight instruments by the comparison method. In the case of the Apollo 17 uv spectrometer we were thus able to select the most efficient optical and electronic components for the flight instrument.

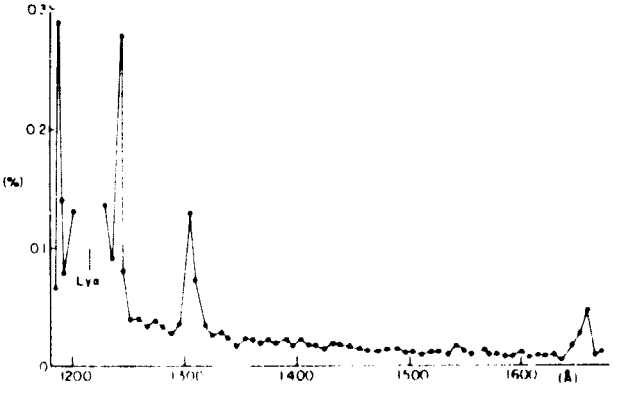

Fig. 3. Measured percentage of scattered Ly α from Apollo 17 flight grating.

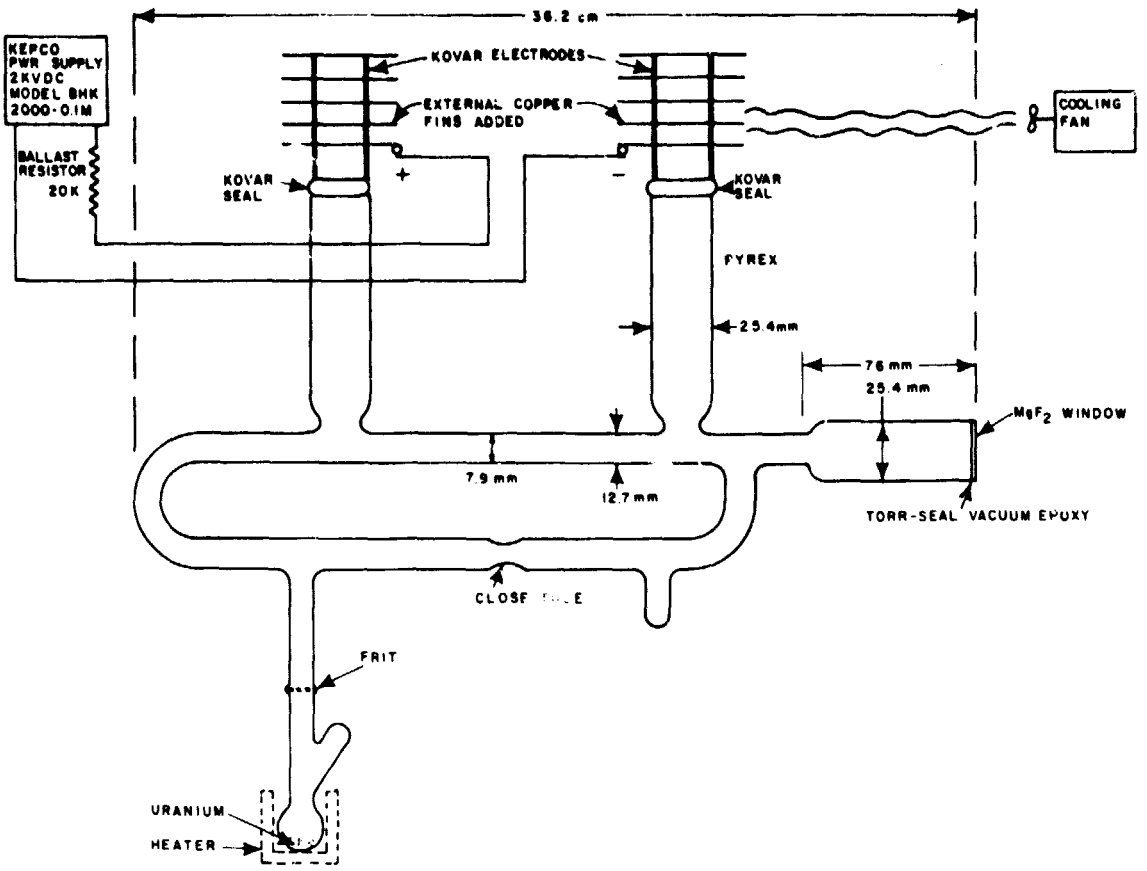

Fig. 4. Far uv molecular hydrogen lamp.

V. Light Source for the Far-Ultraviolet Region

The Apollo 17 calibration program required a light source providing line spectra over a range of wavelengths from 1175 Å to about 1700 Å, which was highly stable for a period of about 1 h and which had emission lines or groups of lines within a 1–10-Å band with radiance of roughly 10^{14} photons sec^{-1} cm^{-2} sr^{-1}. The maximum slit area to be illuminated was 0.25 mm^2, and the f number of the beam was nominally 80. The molecular hydrogen lamp that was developed for this purpose, of which thirty have been made, met these requirements, and because of broadly expressed interest some details of its properties and method of fabrication are presented below.

The possibility of making a lamp of this type rests upon certain peculiarly fortunate chemical and thermodynamic properties of the physical system consisting of uranium + uranium hydride (UH_3) + hydrogen (or any of its isotopes). The basic properties of this system were first investigated by Spedding *et al.*[5] and were used by Dieke and Cunningham[6] and Dieke and Crosswhite[7] to produce high-purity spectroscopic light sources of molecular hydrogen, the rare gases, and metals, the two latter sources employing the properties of U as a getter. The present lamp is a logical extension of this earlier work.

The properties of the uranium–hydrogen system that are important here are the following: (1) uranium metal, when properly prepared in very finely powdered form, is an extremely powerful chemical getter for all gases normally encountered in spectroscopic light sources except the rare gases; (2) the compounds formed between uranium and most elements (hydride, oxide, nitride, etc.) have thermodynamic properties such that the hydride can be formed and dissociated reversibly to yield equilibrium hydrogen pressures useful in discharge light sources (temperatures of 165–227°C give hydrogen pressures from about 0.1 Torr to 2 Torr[5]), while oxides, nitrides, etc. are more tightly bound and require higher temperatures to dissociate them. As a consequence, a mixture of U + UH_3, maintained at temperatures in the range indicated above, can provide a known and controllable pressure of hydrogen, while at the same time any uncombined pure uranium metal serves as a continuously acting effective getter for the other chemically active gases.

The part of the lamp fabrication procedure that is concerned specifically with the uranium is outlined in the Appendix.

The physical form and method of operation of the present lamp are indicated in Fig. 4. The light used for measurement purposes comes from an appreciable length of the positive column of a weak continu-

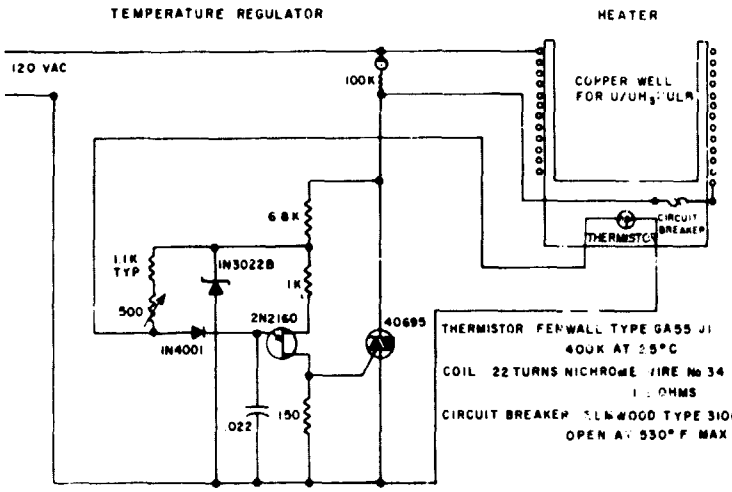

Fig. 5. Temperature regulator and heater for molecular hydrogen lamp.

ous dc discharge, viewed end-on through a MgF_2 (or LiF) window. The lamp current is controlled to better than ±0.05% by a commercially available precision power supply. The temperature of the $U + UH_3$ is controlled, as indicated in Fig. 5, to within approximately ±1°C by a feedback circuit using a thermistor temperature sensor in intimate thermal contact with the electrically heated furnace that surrounds the spherical bulb containing the uranium. The equilibrium temperature is typically about 190°C, corresponding to an equilibrium hydrogen pressure of about 0.36 Torr, although stable operation is possible over a considerable range of both pressure and current.

With the heater control circuit (Fig. 5) set to give a temperature of the uranium bulb of approximately 190°C and lamp current to about 60 mA, the lamp gives a rich spectrum of molecular hydrogen and strong Lyman α at 1216 Å, the latter with some self-reversal. Figure 6 shows a sample scan of parts of the spectrum, taken with a spectrometer resolution of 0.08 Å. The spectrum has been searched carefully between 1200 Å and 1700 Å, and no traces of impurities have been found. There is a small amount of continuum in the 1600–1700-Å region which is due to molecular hydrogen.

The stability of intensity has proven to be impressive; when a precision current-regulated power supply is used and the temperature is controlled as shown, intensity variation of any spectral feature is less than 1%/h. Ordinarily the temperature control circuit is left running continuously. When the lamp

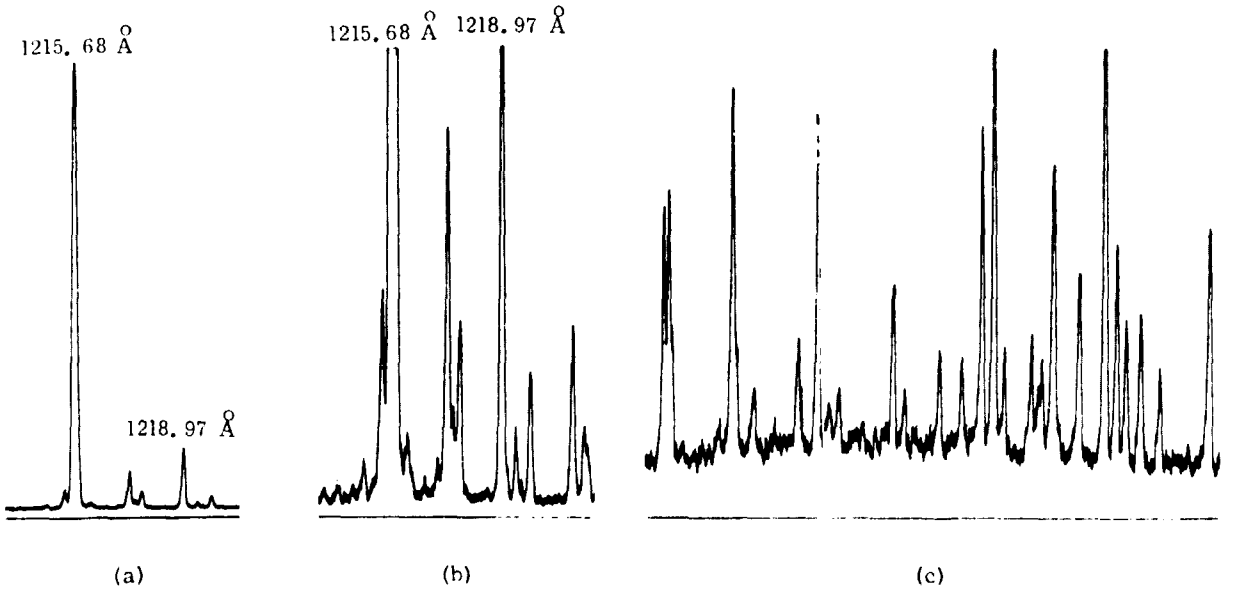

Fig. 6. Sample spectra from the hydrogen lamp; (a) and (b), vicinity of 1216 Å with different amplifier gains; (c) approximately 1570–1590 Å.

is turned off, then turned on again hours or days later at the same current, the light output quickly returns to the same value it had when turned off.

An interesting and unusual feature of this lamp is revealed in the stability and structure of the striations in the discharge, which are particularly striking in the anode and cathode sections of the discharge. At typical operating pressure and current there may be between six and ten bright stationary striations in this region. After several weeks of operation they cause a slight discoloration of the glass in the form of rings, and at constant pressure and discharge current the striations hold this pattern indefinitely. In our experience we have never before encountered such stability of striations.

The operating life of these lamps is not known. Some have operated for thousands of hours, with any degradation of performance or eventual termination due to external mechanical damage—breakage, chipping, or coating of the window with oil in vacuum-system accidents etc. Degradation due to vacuum oil coating[8] of the window can be partially reduced by carefully polishing the outer face of the window with sapphire powder.

We have not specifically investigated the effect of uv radiation from the discharge on the MgF_2 window transmission,[9] but no degradation in spectral transmission has been observed that is not attributable to external effects mentioned above.

VI. Details of Calibration Test Equipment and Procedures

As shown in Fig. 1 the test unit comprises two connected vacuum chambers (a premonochromator chamber and a main chamber that accepts the spectrometer to be calibrated) which are connected by an interface valve 3 in. (7.6 cm) in diameter. Each chamber has a diffusion pump system with well-baffled liquid nitrogen traps and automatic vacuum control circuits, which permit recycling the systems independently from high vacuum to atmospheric pressure and back to a vacuum pressure of 2×10^{-5} Torr in less than 5 min.

The premonochromator chamber has a vacuum fitting by which a uv source can be mounted at the entrance slit of a ¼-m focal length Ebert grating monochromator that has a dispersion of 10 Å/mm. The slits are ¼ mm wide, providing a fixed spectral pass band of 2.5 Å. A manually operated filter wheel at the premonochromator provides cutoff filters at 1250 Å (CaF_2), 1350 Å (BaF_2), and 1650 Å (high purity fused quartz), which are convenient for establishing that the measured signal does not contain scattered light from the more intense long wavelength region of the line source. The exit slit can be adjusted in length to a maximum value of 2.5 mm. The exit beam from the premonochromator goes to the folding mirror M_F, which is fitted with a square limiting diaphragm to provide an $f/80$ beam. The reflected beam goes to the spherical concave mirror M_T, which forms an image of the exit slit at unit magnification in the main chamber at a distance of 1650 mm from M_T. M_T can be adjusted in two axes so that the image can be positioned at any point in the focal plane to within ¼ mm. This adjustment can be made externally either manually or with an electrical drive system that includes two-axis readout dials. The transfer mirror can also be positioned to send the beam to either of the end-on photomultiplier tubes, PMT_A or PMT_B, which are about 3° off the central axis and 800 mm from M_T. Thus the beam illuminates a 10-mm × 10-mm area on the tube faces, which have a diameter of 25 mm. One of the reference tubes has a CsI photocathode with a long-wavelength cutoff at about 1700 Å, the other a CsTe photocathode with a long-wavelength cutoff at about 3000 Å. Both tubes have MgF_2 windows and are mounted on a vacuum cover plate that includes the electrical feedthrough connections for the tubes and interfaces to the vacuum chamber by means of a flange at the top of the premonochromator chamber.

The cover plate also is equipped with a mechanical feedthrough to insert a mirror rhomb in the beam when it is in the central position so that the CsI reference photomultiplier tube (PMT_A) is illuminated. By this means the mirror rhomb reflectivity can be monitored at 1216 Å throughout a calibration test to establish that the vacuum environment or vacuum pumping system is not producing optical contamination.

The main chamber, which receives the spectrometer to be calibrated, has a removable end bell mounted on three plastic wheels that permit rolling the end bell on the table surface of a laminar flow bench. Thus installation in the main chamber can be performed under clean-room conditions.

The flight spectrometer is placed on the gimballed tray in the main chamber with the center of its entrance slit on the central axis of the calibration beam and with the slit in the focal plane of the transfer mirror M_T. The tray is gimballed about horizontal and vertical axes, both of which pass through the center of the entrance slit. External controls with feedthrough mechanical linkages and readout dials are provided so that the spectrometer can be tilted to illuminate any area of the dispersing element with the $f/80$ calibrated beam, with the beam position on the slit being independent of the tilt position to about ±0.25 mm.

The calibrated beam can be positioned at will in the entrance-slit plane. For a given slit position the gimballed tray on which the spectrometer is mounted can be tilted to illuminate various areas of the dispersing element and the spectrometer focusing elements. Large variations in sensitivity along the useful area of the detector at the exit slit of the spectrometer under test or large nonuniformity in the optical efficiency of the dispersing element or focusing elements of the spectrometer disqualify those elements for use in a spectrometer that is to be employed for precision spectroradiometry. Thus in practice, variations in sensitivity along the slit and

across the spectrometer optical elements are relatively small and need to be determined at only a few wavelengths. Measurements at the center of the slit and at the center of the optical system for 10–15 different wavelengths over a 500–1000-Å range are adequate to acquire the needed calibration information.

Most of the instruments that have been calibrated employ entrance and exit slits with a minimum width of 1 mm and a length of 5 mm. Instruments that employ slits with submillimeter widths must have wider slits of the same length substituted for calibration purposes to insure that none of the photons in the calibrated monochromatic beam is cut off by the slits. To insure that no photons are cut off by the entrance or exit slit of the instrument under test, the calibration procedures call for establishing that the instrument output is constant for three positions of the beam between the entrance slit jaws. This check is most conveniently made with the spectrometer scan stopped at the wavelength under study. Once the beam position is thus confirmed, the spectrometer is scanned through its full wavelength cycle as many times as necessary to provide a total output measurement not limited in its accuracy by photon statistics. It is desirable to accumulate a total of about 10^5 photoelectrons at the calibration wavelength so that the spectrum can be studied at all wavelengths for scattered light, false reflections, and grating ghosts.

The reason for emphasis on use of wide slits in the spectrometer under test can be illustrated as follows. In an ideal instrument strictly monochromatic illumination of the entrance slit results in an aberration-free image of the entrance slit being projected onto the exit slit, which is adjusted to have the same width as the image. The energy transmitted through the system vs grating angle is then an equilateral triangle. The width of the triangle is the width of the instrumental response function, and the peak height gives the full transmitted signal at the illuminating wavelength. In an actual situation, because of aberrations in the spectrometer, the images of the edges of the entrance slit will not be perfectly sharp, and the resulting transmission function will be wider, possibly asymmetric, and lower in peak value than the ideal triangle. The total area under the two curves will be the same, however, and this area plus knowledge of the actual slit widths permit calculation of the true peak value of the transmission function. Our experience indicates that effects of aberrations, including slight tilt errors between exit slit and incident image, and slight departures from monochromaticity of illumination jointly leading to essentially triangular functions up to 20% greater than the true width can be used to infer the corrected transmission value.

It might appear that energy lost because of astigmatism or misalignment of the image of the entrance slit on the exit slit in a direction perpendicular to the dispersion would introduce calibration errors. However, radiation occulted by the top or bottom of the exit slit is in fact part of the instrumental transmission function and is thus included in the procedures described here.

The true peak value of the transmission function can also be calculated if the slit widths are small compared to the aberrations or departure from monochromaticity of illumination of the calibration beam, but in this case large errors can be introduced that degrade the accuracy of the calibration. In particular, extreme accuracy would be required of the scan drive mechanism in this case. The grating drive mechanisms for our flight instruments are more than adequate for the wide-slit procedure described above. For example, in one of our recent rocket flights,[10] the Lyman Alpha dayglow feature at 1216 Å showed a peak value of 63 counts with 10-Å physical slit widths, but with a measured 11.5-Å half-width, which gives a true value of 72.5 counts/sec.

Just before a spectrometer calibration, and just afterward, the reference photomultiplier tubes are subjected to calibration in absolute values. A photodiode that has been calibrated at NBS is placed on the tray in the main chamber a distance of 400 mm behind the focal plane of the mirror M_T, so that it is illuminated over a 5-mm × 5-mm area. Preliminary visual observations with the premonochromator grating set in central order and photoelectric scans of the uv beam will have established that the beam illumination is relatively uniform. This is an essential condition because gross nonuniformity across the face of the photodiode or reference photomultiplier tubes could introduce a calibration error.

During the calibration the monochromatic beam is periodically positioned on the appropriate reference photomultiplier tube to confirm that the source output is stable and that the premonochromator wavelength setting is unchanged. Likewise the mirror rhomb is periodically employed to determine that optical contamination has not occurred, and the mirror M_T is scanned across the reference photomultiplier to establish that the standard M_T coordinates for the reference tube have not changed.

On the basis of extensive experience with the detectors and the measuring circuits (Fig. 7) over a period of about 3 years, no error of the magnitude of the uncertainty in the NBS calibration of the diode (±6%) is introduced by the method of calibrating the reference photomultiplier tubes. Tube calibrations before and after a spectrometer calibration always agree to within about 2%, although over a period of a year the reference-tube gain may decrease as a result of total photon exposure by as much as 50%. Likewise, the high-voltage supplies and electrometers are highly stable over the period of several days that may elapse during a spectrometer calibration. Repeated recalibrations of diodes at NBS show only small variations compared to the ±6% photodiode calibration uncertainty. This diode stability has been independently confirmed by repeated calibration of a spectrometer over a period of about a year during which

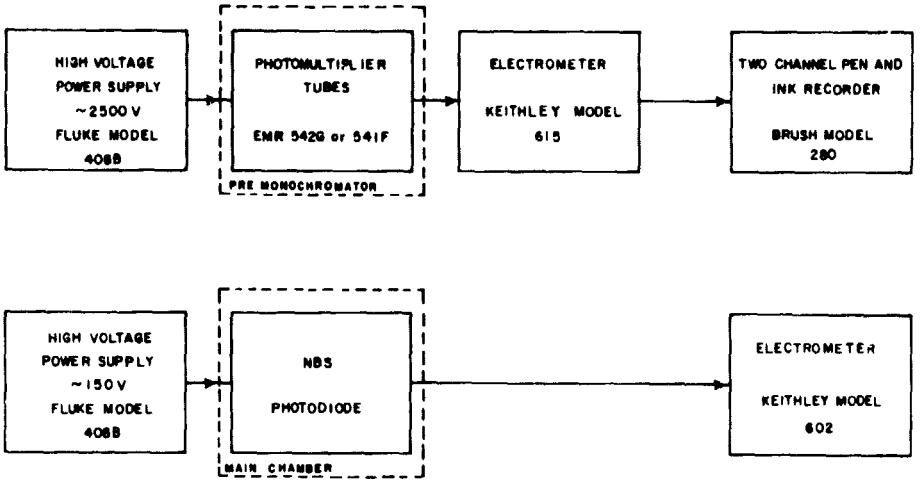

Fig. 7. Calibration facility electronics block diagram (typical).

the spectrometer was sealed in a chamber filled with very dry highly purified nitrogen.

Several modes of operation are required to obtain a precise calibration.

(1) With the premonochromator set at a desired wavelength and with the exit slit image focused on the center of the test spectrometer entrance slit (which is wide enough so that the slit edges do not occult any photons), the test spectrometer is cycled through several wavelength scans.

(2) The premonochromator exit slit image is centered between the jaws of the test spectrometer entrance slit and is slowly scanned from one end of the slit to the other. For this measurement the test spectrometer can be set at the premonochromator wavelength or the test spectrometer can be cycled through its wavelength range to provide readouts at many points along the length of the slit. This observation is necessary to determine the effective length of the entrance slit, which is multiplied by the known physical width of the entrance slits used in flight to determine the entrance slit area (A_s).

(3) With the test spectrometer set at the premonochromator wavelength, the beam is centered on the entrance slit of the test spectrometer. The gimballed plate is set at a number of positions so that the relative signal from many areas of the diffraction grating can be determined. This test is repeated for other positions of the beam on the entrance slit.

(4) The above measurements are repeated for a number of wavelengths.

(5) At a bright spectral line, the lamp current and/or the length of the premonochromator exit slit are varied to permit a determination of the degree of linearity of the detector and/or the detector electronics.

(6) With the premonochromator set at its central order, the test spectrometer is cycled through its wavelength range to determine the wavelength calibration of the wavelength drive mechanism.

An almost completely independent check of the validity of these calibration techniques was obtained by a calibration check of the Apollo 17 prototype spectrometer in the vacuum optical bench at Goddard Space Flight Center, which also uses diodes calibrated at NBS as standards. In the 1350 to 1700-Å spectral range the two calibrations agreed to within the limits set by the diodes. At 1216 Å, a 15–20% discrepancy appeared that was established as being due to the longer vacuum pumping time employed in the Goddard facility. Apparently the degassing of water vapor from the MgF_2-Al coated replica grating or the MgF_2-Al mirrors requires about 10–20 h, during which time the reflectivity at 1216 Å increases. The use of longer pumping times in our facility brought our short wavelength calibration into agreement with the GSFC vacuum optical bench calibration. This experience demonstrates how subtleties can creep into any absolute measurement and suggests that our painstaking efforts to avoid systematic errors were necessary.

VII. Calibration Results

During the preparation of the Apollo 17 uv spectrometer, several calibrations were performed on several instruments over a period of about 1 year. Throughout the testing period, all instruments were stored or transported in special carriers providing an atmosphere of high-purity dry nitrogen, or in a clean-room atmosphere, or in a thermal vacuum chamber. These conditions were also maintained during the testing period at Cape Canaveral and during installation in the spacecraft on the launch pad and throughout the prelaunch period through the launch phase. The flight instrument was installed in the spacecraft on the launch pad just after final calibration 6 weeks before launch. From the time the flight instrument was first calibrated until 48 h before launch, it was always accompanied by a test mirror rhomb whose reflectivity at 1216 Å was tested at intervals in a special fixture in the main chamber of the calibration test equipment. No degradation in the reflectivity of the test rhomb was detected to a limit of ±2%. Table I shows the reproducibility of the calibration of two of the Apollo 17 units at two wavelengths. Table II

Table I. Typical Apollo 17 UVS Calibrations (Normalized to 1.00 at Each Wavelength)

Date	Unit	1463 Å	1608 Å
7 July 72	Flight	1.03	1.02
25 July 72	Flight	1.03	0.99
31 July 72	Flight	0.99	0.99
7 Aug. 72	Flight	0.95	1.01
13 Sept. 72	Flight	0.99	0.99
24 Apr. 72	Backup	0.99	1.04
1 May 72	Backup	0.99	1.03
22 May 72	Backup	1.02	0.94
25 May 72	Backup	1.00	1.01

Table II. NBS Diode Calibrations (Normalized) Diode 17195—CsI Photocathode

Date	1216 Å	1608 Å
17 Nov. 71	0.97	0.99
23 March 72	1.00	0.99
6 Nov. 72	1.01	0.99
27 March 74	1.01	1.02

shows the reproducibility of the NBS diode on successive recalibrations at NBS. The repeatability of these calibrations, the maintenance of a benign atmosphere through the launch phase, and the monitoring of the reflectivity of the test rhomb provide high confidence in the absolute accuracy of the radiometric results.

One of the experimental results of the Apollo 17 UVS mission was the measurement of the absolute brightness of several stars.[10] We believe, because of the techniques described above, that these measurements provide the most accurate existing uv stellar spectral radiance measurements for these stars.

The calibration facility was designed and constructed by Ray Lee Instruments, Pikesville, Md. The Applied Physics Laboratory of The Johns Hopkins University was responsible for the Apollo 17 flight hardware and provided support for the calibration operations and the field operations. James Diggins provided the cross calibration in the Goddard Space Flight Center Vacuum Optical Bench and also assisted in many facets of the program. Robert Richardson was responsible for final installation and operation of the Calibration Facility. Robert C. Schaeffer conducted the calibration of all the Apollo units. Edward Reed performed the flight simulation test during the mission with a spare instrument. The uv standards group at NBS calibrated the reference diodes under the direction of Robert P. Madden.

The development of the calibration techniques described herein was supported by NASA grant NGR 21-001-001. Construction of the calibration facility and support of the Apollo 17 spectrometer calibration was financed by NASA contract NAS 9-11528.

Appendix: Preparation of Uranium–Uranium Hydride Powder

The part of the lamp fabrication procedure concerned specifically with the uranium can be sketched as follows. About 1.2 g of pure uranium chips, turnings, or slivers cut from a thin uranium sheet are carefully cleaned in warm dilute HNO_3 to remove the surface oxide, washed thoroughly in distilled water and dried, and put into the lamp's small spherical container before appreciable oxide has reformed (½ h). The lamp is sealed onto the vacuum system and pumped to about 10^{-6} Torr, while the uranium bulb is heated by a small electric oven to about 200°C to drive off all moisture. The uranium is cooled to room temperature, and hydrogen is admitted to a pressure just under 1 atm. (The highest purity of hydrogen is not necessary, but it should be free of water.) The temperature of the oven is very slowly increased, while the pressure in the system is observed on an accurate pressure gauge. At temperatures of roughly 130°C a pressure drop indicates the beginning of the conversion of the metallic uranium to the hydride. Depending upon the rate of change of temperature and the size and surface state of the uranium particles, only part of the uranium is converted to the hydride in this first step; consequently the oven temperature should be raised and lowered slowly between roughly 100°C and 270°C several times until the minimum pressure is approximately constant; as emphasized by Spedding,[5] carrying this step (or the later ones) to completion may require at least 48 h. Usually 4 h is sufficient to achieve roughly 80% of any of the reactions involved, and, because the quantity of uranium used is more than adequate, it is seldom worth the time to attempt totality of any of the reactions. One gram of uranium requires 0.15 liter-atm of H_2 for complete conversion to UH_3. It is convenient to provide sufficient volume in the gas-handling system so that the minimum pressure does not drop below about ½ atm, because the reaction rate depends fairly strongly on excess hydrogen pressure.

After conversion to the hydride is complete, the lamp could be used as a hydrogen source with no further changes, but, because the gettering action of pure uranium is also desired, part of the hydrogen must be driven off. The shape of the curves, representing equilibrium dissociation pressure of hydrogen[5] over $U + UH_3$, suggests that U and UH_3 be provided in roughly equal amounts. Consequently the oven temperature is raised to about 430°C and held for several hours, when the UH_3 will be mostly dissociated, leaving pure uranium metal and hydrogen, at a pressure essentially equal to the initial cold filling pressure. (It is advisable to vary temperature between about 100°C and 430°C several times, waiting several hours at each end of the cycle, until the corresponding total change in hydrogen pressure ΔP is essentially constant.) This value of ΔP is a direct measure of the quantity of hydrogen required to convert the uranium completely to the hydride. The

last step is to raise the oven temperature to 430°C, wait for the pressure to stabilize, pump off enough hydrogen to drop the pressure by $\Delta P/2$, cool to room temperature, and seal the lamp off the vacuum system. The uranium bulb then contains a mixture of approximately 50% uranium metal and 50% uranium hydride in the form of a dark brown or black powder of extremely fine particles. A small electrical heater with a temperature controller is then permanently installed on the spherical bulb. Care should be taken in handling the lamp, for if the processed uranium is exposed suddenly to air it burns to form a fine powder of uranium oxide that should not be breathed.

The final touches to the above manuscript were performed by D. E. Kerr the day before surgery which discovered that he had terminal cancer. He responded to the referees' comments during his final days. The surviving author wishes to point out that Professor Kerr was the major contributor to the development of the molecular hydrogen discharge tube, which is a critical component of the calibration system.

References

1. W. G. Fastie, Moon **7**, 49 (1973).
2. W. G. Fastie, P. D. Feldman, R. C. Henry, H. W. Moos, C. A. Barth, G. E. Thomas, and T. M. Donahue, Science **182**, 710 (1973).
3. W. R. Ott, P. Fieffe-Prevost, and W. L. Wiese, Appl. Opt. **12**, 1618 (1973).
4. L. R. Canfield R. G. Johnson, and R. P. Madden, Appl. Opt. **12**, 1611 (1973).
5. F. H. Spedding, A. S. Newton, J. C. Warf, O. Johnson, R. W. Nottorf, I. B. Johns, and A. H. Daane, Nucleonics **00** (1), 4 (1949).
6. G. H. Dieke and S. P. Cunningham, J. Opt. Soc. Am. **42**, 187 (1952).
7. G. H. Dieke and H. M. Crosswhite, J. Opt. Soc. Am. **42**, 433 (1952).
8. R. G. Taylor, T. A. Chubb, and R. W. Kreplin, J. Opt. Soc. Am. **55**, 1078 (1965).
9. P. Warneck, J. Opt. Soc. Am. **55**, 921 (1965).
10. W. G. Fastie, Appl. Opt. **11**, 1960 (1972).
11. R. C. Henry, A. Weinstein, P. D. Feldman, W. G. Fastie, and H. W. Moos, Low-Resolution Ultraviolet Spectroscopy of Several Hot Stars from Apollo 17, accepted by Astrophys. J. (1975).